Histone variant H2B.Z acetylation is necessary for maintenance of *Toxoplasma gondii* biological fitness

Laura Vanagas[1*], Daniela Muñoz[1], Constanza Cristaldi[1], Agustina Ganuza[1], Rosario Nájera[1], Mabel C. Bonardi[1], Valeria R. Turowski[2], Fanny Guzman[3], Bin Deng[4], Kami Kim[5], William J. Sullivan Jr.[6] and Sergio O. Angel[1*]

[1]Laboratorio de Parasitología Molecular, INTECH, CONICET-UNSAM, Av. Intendente Marino Km. 8.2, C.C 164, (B7130IIWA), Chascomús, Prov. Buenos Aires, Argentina.

[2]Laboratorio de Bioquímica y Biología Celular de Parásitos, INTECH, CONICET-UNSAM, Av. Intendente Marino Km. 8.2, C.C 164, (B7130IIWA), Chascomús, Prov. Buenos Aires, Argentina.

[3]Núcleo de Biotecnología Curauma, Pontificia Universidad Católica de Valparaiso. Av. Universidad 330 Curauma, Valparaiso

[4]Department of Biology and VBRN, University of Vermont, Vermont, USA.

[5] Department of Internal Medicine, Morsani College of Medicine, University of South Florida, Tampa, FL 33612

[6] Department of Pharmacology and Toxicology, Indiana School of Medicine, Indianapolis, Indiana 46202, USA

*Corresponding authors: Sergio O. Angel. Laboratorio de Parasitología Molecular, IIB-INTECH, CONICET-UNSAM, Av. Intendente Marino Km. 8.2, C.C 164, (B7130IIWA), Chascomús, Prov. Buenos Aires, Argentina. Tel.: +542241424303

E-mail address: sangel@intech.gov.ar (SO Angel)

Laura Vanagas. Laboratorio de Parasitología Molecular, IIB-INTECH, CONICET-UNSAM, Av. Intendente Marino Km. 8.2, C.C 164, (B7130IIWA), Chascomús, Prov. Buenos Aires, Argentina. Tel.: +542241424303

E-mail address: vanagas@intech.gov.ar (L Vanagas)

Abstract

Through regulation of DNA packaging, histone proteins are fundamental to a wide array of biological processes. A variety of post-translational modifications (PTMs), including acetylation, constitute a proposed histone code that is interpreted by "reader" proteins to modulate chromatin structure. Canonical histones can be replaced with variant versions that add an additional layer of regulatory complexity. The protozoan parasite *Toxoplasma gondii* is unique among eukaryotes in possessing a novel variant of H2B designated H2B.Z. The combination of PTMs and the use of histone variants is important for gene regulation in *T. gondii,* offering new targets for drug development. In this work, *T. gondii* parasites were generated in which the 5 N-terminal acetylatable lysines in H2B.Z were mutated to either alanine (c-Myc-A) or arginine (c-Myc-R). c-Myc-A mutant only displayed a mild effect in its ability to kill mice. c-Myc-R mutant presented an impaired ability to grow and an increase in differentiation to latent bradyzoites. This mutant line was also more sensitive to DNA damage, displayed no virulence in mice, and provided protective immunity against future infection. While nucleosome composition was unaltered, key genes were abnormally expressed during *in vitro* bradyzoite differentiation. Our results show that the N-terminal positive charge patch of H2B.Z is important for these procceses. Pull down assays with acetylated N-terminal H2B.Z peptide and unacetylated one retrieved common and differential interactors. Acetylated peptide pulled down proteins associated with chromosome maintenance/segregation and cell cycle, opening the question of a possible link between H2B.Z acetylation status and mitosis.

Key words: *Positive charge patch – cell cycle – differentiation – virulence – mitosis*

46 # Introduction

47 Histones proteins function to form nucleosomes that regulate packaging of DNA, thereby affecting
48 DNA transcription, replication, and repair. In addition to the four canonical histones (H2A, H2B, H3 and H4),
49 variant histones exist that can be substituted into the nucleosome, affecting its properties. Canonical and
50 variant histones are also subject to a wide array of post-translational modifications (PTMs) that can alter
51 the nucleosome or recruit chromatin remodeling machinery. The combination of PTMs and exchange of
52 histone variants is believed to be important for gene regulation in the protozoan parasite *Toxoplasma*
53 *gondii,* offering new targets for drug development [1-3].

54 *T. gondii* is a member of phylum Apicomplexa and infects between 10-90% of the population
55 depending on the country [4], presumably influenced by dietary habits and environmental conditions [5].
56 *T. gondii* converts from rapidly growing tachyzoites, which cause acute infection, to slow or non-growing
57 bradyzoites, which cause chronic infection and typically reside in the brain [6]. Although *T. gondii* infection
58 is asymptomatic in healthy people, untreated clinical toxoplasmosis can be lethal in immunocompromised
59 individuals such as transplant or HIV patients, and can produce severe disease during congenital infection,
60 especially in early stages of development [7, 8]. Chronic toxoplasmosis has also been linked to brain tumor
61 predisposition, attention-deficit/hyperactivity disorder, obsessive-compulsive disorder and schizophrenia
62 [9-13].

63 The *T. gondii* life cycle is comprised of sexual and asexual stages. While sexual replication takes
64 place only in felids, *T. gondii* is able to replicate asexually as tachyzoites in any nucleated cell in any warm-
65 blooded vertebrate. Following infection, tachyzoites convert into bradyzoites, which are house in tissue
66 cysts that are impervious to immunity and current drug treatments. Recently, a myb-like transcription
67 factor (BFD1) was described to be necessary and sufficient to induce bradyzoite differentiation [14]. How
68 BFD1 is recruited to stage-specific promoters remains to be determined, but likely involves interplay with

69 chromatin remodelers and epigenetic processes that include histone PTMs and/or variant histone exchange
70 [15]. In support of this idea, treatment of tachyzoites with inhibitors of histone deacetylase 3 (HDAC3)
71 initiates bradyzoite differentiation [16]. The roles of histone variants in *T. gondii* remain poorly understood.

72 *T. gondii* expresses histone variants that we have previously shown mark functional regions of the
73 genome [17]. H2A.Z is a ubiquitous variant that has been implicated in both transcriptional activation and
74 gene silencing in eukaryotes, and in fine regulation of important processes as DNA damage repair [18-20],
75 which is also present in *T. gondii* [21]. Unlike H2A.Z, only specialized isoforms of the H2B histone family
76 have been described in nature, except for apicomplexan parasites [22-25] and trypanosomatids [26], in
77 which a H2B.Z and a H2Bv variants, were identified, respectively.

78 Histones H2A.Z and H2B.Z form a dimer that localizes with the transcriptional activation mark
79 H3K4me3 in promoter/transcriptional start site (TSS) regions surrounding the nucleosome-free region
80 upstream of the transcription start site [17]. In addition, H2B.Z and H2A.Z histones localize to the gene
81 bodies of silent genes, including repressed stage-specific genes, suggesting a role in the regulation of stage
82 transitions. In *T. gondii*, both H2A.Z (TGGT1_300200) and H2B.Z (TGGT1_209910) are essential during the
83 lytic cycle with CRISPR fitness scores of -5.08 and -4.05, respectively [27]. By mass spectrometry, both
84 histone variants were found to be hyperacetylated at the N-terminal domain, whereas few or no acetylation
85 marks were identified on canonical H2A, H2B and H2A.X [28]. *T. gondii* H2B.Z was shown to be acetylated
86 at 5 lysine residues in its N-terminal tail. The H2A.Z N-terminal tail has 10 acetylatable lysines, in which
87 lysine 18 can also be methylated [28]. H2A.Z N-terminal tail acetylation has been widely shown to be a
88 hallmark for active chromatin whereas N-terminal methylation is associated with gene silencing [29-32],
89 suggesting it is essential for changes in gene expression during cell differentiation [33-37]. While the role
90 of N-terminal lysine acetylation in H2B.Z has not yet been studied, N-terminal acetylated canonical H2B is
91 associated with some, but not all, active genes in vertebrates [38]. Interestingly, H2A.Z in most eukaryotes
92 only bears 4-5 acetylatable lysine residues in the N-terminus, while in protists like *T. gondii, Plasmodium* or

93 *Tetrahymena termophila,* this number is considerably higher (between 5 and 16). Moreover, the presence
94 of a *T. gondii* double variant nucleosome that altogether carries 15 acetylatable lysines that could be
95 regulated is highly intriguing.

96 In the present work we studied the role of the five *T. gondii* H2B.Z N-terminal tail lysines, using a
97 mutagenesis strategy; we also pursued a gene knockout strategy for H2B.Z. In an RH strain background, we
98 generated *T. gondii* that possess mutated versions of H2B.Z: c-Myc-R, in which the five N-terminal
99 acetylatable lysines were replaced by arginines, and c-Myc-A, in which they were replaced by alanines.
100 These lines were analyzed for their ability to grow *in vitro*, differentiate to bradyzoites *in vitro* and produce
101 virulence in mice. In addition, expression of key genes was studied, as well as nucleosome composition and
102 DNA damage sensitivity. Our results suggest that regulation of the N-terminal positive charge patch by
103 lysine acetylation, rather than the histone code, is essential for the aforementioned biological processes.
104 We have also found some differential interactors for an acetylated N-terminal H2B.Z peptide, compared to
105 a unacetylated one, opening new questions on the function of this modification and this histone variant.
106 The implications of these data on the putative role of H2B.Z is discussed.

107

108 # Results

109 **Sequence alignment of Apicomplexa H2B.Z N-tail**

110 H2B.Z is a variant histone of the H2B family that appears early in the phylum Apicomplexa.
111 Previously, it was observed that *T. gondii* and *Plasmodium falciparum* H2B.Z N-terminal tails contain five
112 acetylated lysines (K4,K9,K13,K14 and K18) [28, 39, 40]. The conservation of the five acetylatable lysines is
113 clear from the alignment of H2B.Z N-terminal tail sequences from different Apicomplexa (Fig. 1A). This
114 profuse number of modifications in the N-terminal tail, concomitant with the nucleosome partner, H2A.Z,

115 in which several acetylatable lysines are present, make this double variant nucleosome a likely feature for
116 chromatin modification relevant to gene expression, replication and/or DNA damage responses.

117

118 **Overexpression of tagged wild type and mutant versions of H2B.Z and Knock out of endogenous *H2B.Z***

119 Attempts to obtain a mutant cell line by deletion of the *h2b.z* gene were unsuccessful (data not
120 shown). The failure to obtain an H2B.Z. knockout is consistent with its CRISPR fitness score of -4.05, strongly
121 suggesting it is essential [27] (ToxoDB, TGGT1_209910).

122 Given the high number of modifiable lysines in the H2B.Z variant unique to apicomplexan parasites,
123 we analyzed their role by using an over-expression strategy of myc-tagged wild-type or mutant forms. We
124 generated parasites over-expressing wild-type H2B.Z (c-Myc-WT-OE) or a mutated form in which all the
125 acetylatable lysines in the N-terminal tail were changed to alanine, which mimics how acetylation ablates the
126 positive charge of the lysine residues. We also over-expressed a mutated version in which the lysines were
127 replaced with arginines, which would generate a constitutive positive charge patch but no longer support
128 acetylation (Fig. 1B). Neither mutant form would be acetylated in this region, therefore would be incapable
129 of interacting with bromodomain containing proteins. Correct localization of each c-Myc-H2B.Z protein was
130 checked by immunofluorescence assay (IFA) (Fig. S1A) and by western blotting, observing two bands in every
131 over-expressing line (Fig. S1B). To note, c-Myc-WT-OE was already used in a ChIP seq screen, showing the
132 same genomic localization as endogenous H2B.Z when the experiments were performed using α-H2B.Z
133 antibody [17].

134 After that, endogenous *H2B.Z* gene was deleted by using CRISPR methodology in the previously
135 generated *T. gondii* lines overexpressing mutant H2B.Z versions (Fig 2A). We took advantage of the number
136 of mutations in the N-terminal tail of the tagged version to design sgRNA specific for endogenous *H2B.Z* gene.
137 By this strategy, we obtained *T. gondii* RH lines only expressing c-Myc-tagged H2B.Z with N-terminal

138 mutations, which were named c-Myc-A and c-Myc-R (Fig. 2A-C, Fig. S1C-D). Each form of c-Myc H2B.Z in these
139 parasites localized properly to the nucleus (Fig. 2B). In both CRISPR manipulated clones, a single band
140 corresponding to c-Myc-tagged mutated H2B.Z can be observed by western blot with anti-H2B.Z and anti-c-
141 Myc antibodies (Fig. 2C). Quantification of the band corresponding to c-Myc H2B.Z relativized to Sag1 as a
142 charge control, was 1.43 ± 0.77 and 1.65 ± 0.82 for c-Myc-R and c-Myc-A, respectively, indicating comparable
143 levels of expression between both mutants.

144

145 ***In vitro* growth analysis in c-Myc-R and c-Myc-A *T. gondii* lines**

146 We used a competitive growth assay to determine differences in parasite growth between parental
147 wild-type and mutant parasites (c-Myc-A and c-Myc-R) obtained, which could be distinguished by the c-Myc
148 tag. Approximately equal amounts of c-Myc positive and c-Myc negative (parental) tachyzoites were mixed
149 and allowed to invade hTert cells, which were analyzed by IFA on different days post-infection. While the c-
150 Myc-A parasites showed no change in growth relative to the parental line over time, the c-Myc-R line showed
151 a marked growth deficiency compared to the parental line (Fig. 3A). As arginines conserve the positive charge
152 but cannot be acetylated, these results indicate that the constitutive positive charge patch on the H2B.Z N-
153 terminal tail, but not the lack of acetylation, impairs tachyzoite growth *in vitro*. Therefore, wild-type *T. gondii*
154 must regulate the charge patch on H2B.Z N-terminal tail by PTMs such as acetylation for normal growth.

155

156 ***In vitro* differentiation analysis in c-Myc-R and c-Myc-A *T. gondii* lines**

157 We next studied the effect of the mutant H2B.Z variants on *in vitro* tachyzoite to bradyzoite
158 differentiation using alkaline stress to trigger stage conversion and *Dolichos biflorus* lectin (DBL) to monitor
159 tissue cyst wall formation. Strikingly, we found that c-Myc-R, but not c-Myc-A, showed an increase in DBL-

160 positive vacuoles compared to the wild-type control (Fig. 3B), suggesting that the impossibility to regulate
161 the presence of a positive charge patch in the H2B.Z N-terminal tail promotes an *in vitro* differentiation.

162 We also checked whether key stage-specific genes were altered in parasites expressing mutant
163 H2B.Z. We obtained RNA from freshly lysed tachyzoites, early bradyzoites (48 hours post-differentiation),
164 and late bradyzoites (96 hours post-differentiation) of the parental RH strain and c-Myc-A or c-Myc-R
165 parasites. We analyzed the expression of *Sag1* (tachyzoite), *Bag1* (early bradyzoite), *LDH2* (early bradyzoite),
166 *AP2IX-9* (mature bradyzoites) [41], *AP2 IV-3* (in which expression is maximal at 48h post- differentiation,
167 decreasing in mature bradyzoites) [42] and *BFD1* [14] mRNA by RT-qPCR. Actin and Tubulin were used as
168 housekeeping genes, and data were normalized to actin. The amount of expression relative to tachyzoite in
169 each parasite line is plotted, showing a trend of expression in c-Myc-R similar to what would be expected for
170 a cystogenic strain with the treatment, and different from RH expression profile (Fig. 3C). Also, the expression
171 of *BFD1* showed an increase in c-Myc-R, compared to RH (Fig. 3C). Notably, the expression profile of BFD1 in
172 RH type I strain has not been published to date. These results are consistent with the heightened bradyzoite
173 differentiation rate seen in c-Myc-R parasites.

174

175 **Sensitivity to DNA damaging agents in c-Myc-A and c-Myc-R lines**

176 In other species, H2A.Z has been linked to double strand break repair driven by the non-homologous
177 end joining (NHEJ) pathway [20, 43, 44]. Consequently, H2A.Z is associated as a responder to HU or MMS
178 genotoxic effects [44]. We have previously characterized the anti-*T.gondii* effect of MMS, HU, and
179 campothecin [45]. Topotecan is a genotoxic drug analog to campthotecin that produces fork collapse, and
180 ulterior DNA double strand break repaired by HRR [46].

181 Given the roles of histone variants in DNA repair, we analyzed c-Myc-A and c-Myc-R parasites for
182 sensitivity to topotecan at its IC_{50} value (20 μM, unpublished results) and MMS (50 μM) using the competitive

183 growth assay. We observed a significative decrease in growth compared to the parental after treatment only
184 with MMS for c-Myc-R tachyzoites (Fig. 4A). By contrast, topotecan did not produce a significant defect in
185 growth, although c-Myc-R seems to be more sensitive (Fig. 4A). In addition, treatment with MMS produced
186 a disorganization of vacuoles, rounded shapes and a loss of genetic material in both mutants as well as
187 parental (Fig. 4B). *T. gondii* normally presents a synchronic replication in the parasitophorous vacuole (PV).
188 As a result, PVs usually show 2, 4, 8, 16 and so on, tachyzoites (Tz) per PV. Treatment with MMS and
189 Topotecan also caused a loss of synchronization, with an altered number of Tz per PV, which was also counted
190 as "anomalous vacuole". Anomalous vacuoles and loss of genetic material were also observed with topotecan
191 treatment (Fig. 4B). However, quantification showed that anomalous PV are significantly more abundant in
192 c-Myc-R than parental and c-Myc-A, with both drugs tested (Fig. 4C). Taken together, the constitutive positive
193 charge patch generated in the c-Myc-R parasites alter the DNA damage response after MMS treatment,
194 suggesting that acetylation status of H2B.Z N-terminal tail is likely to be modulated for proper DNA repair.

195

196 ***In vivo* analysis in c-Myc-R and c-Myc-A *T. gondii* lines**

197 Proper gene regulation is required for tachyzoite propagation in different tissue environments and
198 differentiation *in vivo*. Progression of tachyzoite infection of these mutants was analyzed in C57BL/6 mice by
199 inoculating 100 tachyzoites per *T. gondii* line. As expected, parental parasites displayed high virulence, killing
200 mice within 7 days (Fig. 5A). c-Myc-A tachyzoites were also lethal to mice, but with a delay in the time of
201 death (Fig. 5A). According to Mantel-Cox and Gehan-Breslow-Wilcoxon tests, the survival curves are
202 significantly different ($p>0.0001$), suggesting that acetylation of at least some of the 5 N-terminal tail lysines
203 is relevant for parasite progression *in vivo*.

204 In contrast, c-Myc-R and Me49 infected mice, as well as non-infected (PBS group) survived until
205 sacrifice on day 30-35 (Fig. 5A). c-Myc-WT-OE was used a control that the tagged version is not responsible

206 *per se* of any affect observed. *T. gondii* line expressing both endogenous H2B.Z and c-Myc-H2B.Z-R (c-Myc-R-
207 OE) previous to CRISPR procedure, were as lethal as the parental line (data not shown), suggesting that the
208 randomly integrated ptub-*H2B.Z-R* gene is not responsible for the loss of virulence and that co-expression of
209 H2B.Z wt and H2B.Z-R mutant histone did not generate a dominant negative *T. gondii* line. Infection with
210 1,000 and 10,000 c-Myc-R tachyzoites were also nonlethal to mice (Fig S2A).

211 To confirm acute infection took place, hematoxylin and IFA staining of the peritoneal fluids at day 4
212 post-infection were performed (Fig. 5B). Intraperitoneal tachyzoites could be detected only with parental
213 and c-Myc-A *T. gondii* lines infections, but not with c-Myc-R parasites (Fig. 5B). Surviving animals (c-Myc-R
214 and Me49 *T. gondii* lines) were analyzed to detect antibodies against *T. gondii*. An increase in total IgG in
215 mice infected with c-Myc-R tachyzoites was observed, comparable to Me49, which indicated that an initial
216 infection had taken place (Fig. 5C, Fig. S2B). The analysis of IgG subtypes showed a Th1-like humoral response
217 in both cases, associated to IgG2a and higher for IgG2b (normal for C57/BL6 mice), typical for an intracellular
218 parasite infection (Fig. 5C, Fig. S2B). Following sacrifice, brains of surviving mice were processed for cyst
219 detection by direct observation with optical microscopy and DBL staining. Tissue cysts were observed in
220 brains of mice infected with Me49 strain, but not in those infected with c-Myc-R parasites (data not shown).

221 To determine if infection with c-Myc-R parasites elicits an adequate immune response, mice
222 previously infected with 1,000 c-Myc-R tachyzoites were reinfected with 100 tachyzoites of the highly virulent
223 RH parental line. c-Myc-R infected mice survived until sacrifice, while all mice in the control group died at day
224 38 (day 8 after re-infection) (Fig. 5D). These results suggest that c-Myc-R tachyzoites must have been capable
225 of invading cells and producing a stimulation of the cellular immune response adequate to control a challenge
226 infection before clearing.

227

228 **H2B.Z acetylation status is involved in regulation of ROP proteins expression**

229 The ability of the c-Myc-R line to establish a protective immune response suggest these parasites can
230 invade the host cells but are efficiently controlled by the immune system. Among the *T. gondii* virulence
231 proteins that exert protection from PV establishment are the polymorphic rhoptry proteins Rop5 and Rop18,
232 which disrupt the γIFN-inducible IGR pathway [47-51]. Here, we used antibodies against *T. gondii* Rop5
233 (TGGT1_411430) and Rop18 (TGGT1_205250) recombinant proteins for western blot analysis. Rop5 was
234 present in parental, c-Myc-A, and c-Myc-R parasites, whereas Rop18 only in the parental line (Fig. 6A).
235 However, quantification of the band intensities showed a significative decrease in Rop5 abundance in c-Myc-
236 R parasites and a lack of Rop18 protein in both c-Myc-A and c-Myc-R (Fig. 6B and Fig. S3A). To test whether
237 the absence of Rop18 was a consequence of the insertion of the H2B.Z construction in that locus, we
238 performed the same experiment using the over-expressing tachyzoites obtained prior to CRISPR
239 manipulation. As shown in Fig.S3 (B, C) both Rop5 and Rop18 are detectable in every clone similar to parental.
240 Co-localization analysis showed a correct localization of Rop5 in all *T. gondii* lines whereas Rop18 could only
241 be detected in the parental line (Fig. 6C). Of note, we also detected a decrease in the fluorescence intensity
242 of Rop5 in c-Myc-R parasites (Fig. 6D). RT-PCR analysis indicated that both genes were expressed in every *T.*
243 *gondii* line (Fig. S3D), suggesting that alteration of Rop5 and Rop18 expression in the c-Myc-R line is likely at
244 the post-transcriptional level.

245

246 **Double variant nucleosome and transcription is not altered in *T. gondii* mutant lines in normal conditions**

247 Since H2BZ is part of the double variant nucleosome with H2AZ, which localizes at the promoter
248 region of active genes, it was expected that expression alterations would occur at the transcriptional level
249 rather than post-trancriptionally. To determine if the observations for Rop5 and Rop18 were a specific
250 situation, we looked closer at the role of H2B.Z in transcription. We first analyzed the double variant
251 (H2A.Z/H2B.Z) formation in both mutant lines by co-immunoprecipitation (co-IP) assays by using commercial

252 anti-c-Myc agarose. Mononucleosomes of c-Myc-A and c-Myc-R lines were obtained after MNAse digestion
253 before co-IP (Fig. 7A). In figure 7B it can be observed that both c-Myc-A and c-Myc-R H2B.Z interact with
254 H2A.Z, confirming the assembly of the double variant nucleosome already found in *T. gondii*. We also decided
255 to study the interaction of the double variant nucleosome with acetylated H3, a known mark of active
256 chromatin. Both c-Myc-A and c-Myc-R H2B.Z interacted with this acetylated histone, which indicates that lack
257 of acetylation of H2B.Z does not alter this PTM crosstalk (Fig. 7B and Fig. S4). Quantification of the IP band
258 intensities relative to the respective input band showed that both *T. gondii* lines exhibit similar interaction
259 levels with H2A.Z and acetylated H3 (Fig. 7C). These data indicate that the double variant nucleosome was
260 not altered as well as its interaction with an open chromatin marker (acetylated H3).

261 We next decided to explore if transcription was altered in tachyzoites of the mutant lines. We
262 analyzed expression of *Sag1* (tachyzoite), *tubulin* (constitutive), *Bag1* and *LDH2* (bradyzoite) and *BFD1*
263 (master differentiation factor). Only BFD1 mRNA expression was statistically higher in c-Myc-R that in the
264 parental or c-Myc-A (Fig. 7D), consistent with our observation that c-Myc-R parasites are more prone to
265 differentiate into bradyzoites.

266

267 **Chromatin compaction does not explain differences observed in *T. gondii* mutant lines**

268 The positive charge patch on H2B.Z could be associated with a more compact chromatin structure.
269 Since the mark of H2B.Z, either wild type or mutants, and DAPI are coincident in the diameter of the nucleus,
270 to analyze chromatin compaction, we measured the size of the nuclei of these lines compared to the parental
271 in IFAs stained with α-H2B.Z antibody. As shown in Fig. 7E, nuclei sizes are significantly smaller that the
272 parental in c-Myc-R parasites in accordance with the hypothesis. However, this significant difference is also
273 seen in c-Myc-A tachyzoites, indicating that the inability of this histone to be post-translationally modified is
274 enough to lead to this state. The sizes of c-Myc-WT-OE parasite nuclei were similar to parental nuclei,

275 suggesting that the c-Myc tag is not responsible for the effect observed (Fig. 7E). Taken together, acetylation
276 of the H2B.Z N-terminal tail is required for proper control of DNA compaction status.

277

278 **H2B.Z interacting proteins**

279 While results largely implicate the positive charge patch of H2B.Z N-terminal tail as responsible for the
280 observed phenotypes, a role for acetylation cannot be ruled out. Acetylation may explain why the c-Myc A
281 line showed a mild defect in virulence *in vivo* and defects in chromatin compaction. These defects could be
282 associated with the interaction with acetylation "reader" proteins. We therefore examined if there are
283 differential proteins interacting with H2B.Z N-terminal region depending on its acetylation state. We
284 designed two peptides, one containing two acetylated lysines (K14 and K18) and the other unacetylated;
285 both peptides contained a biotin tag towards the C-terminal end (Fig. 8). Peptide design was performed
286 according to Wysocka 2006 [52]. In this work, it was recommended to perform the synthesis of peptides
287 about 20 amino acids long, with biotin conjugated through a linker on the C-terminus for N-terminal histone
288 peptides, and with the modification positioned close to the center of the peptide. In addition, two
289 consecutive modifications were not recommended, explaining our choice of K14 and K18.

290 We used extracellular tachyzoites (RH) to perform the pull-down assays. After resolving on SDS-
291 PAGE, samples were analyzed by mass spectrometry. We detected a total of 48 interactors, 18 exclusive of
292 non-acetylated oligo, 17 exclusive of acetylated oligo and 14 present in both (Table S1). While many
293 interactors have nuclear localization, other localizations were detected, and many typical contaminants (e.g.
294 ribosomal subunits). Among the nuclear proteins, we can select a few that can be interacting with the H2B.Z
295 N-terminal tail independent of acetylation status; among them, GCN5-A, histone H4 and a PHD protein (Fig.
296 8). Interestingly, only three nuclear proteins were differentially pulled down with strong evidence (2
297 independent pull downs), one of them TGME49_262620, a RRM protein (unacetylated peptide), H3.3 and a

298 putative CDK protein (both with the acetylated peptide). Considering the nuclear genes that only appeared
299 in 1 pull down, the acetylated peptide retrieved only genes that code for proteins associated with the
300 maintenance and segregation of chromosomes during the cell cycle, as peptidase c50 (TGME49_262825),
301 RecF/RecN/SMC N terminal domain-containing protein (TGME49_231170) and meiotic recombination
302 protein DMC1 family (TGME49_216400) (Table S1). Among the retrieved peptides in both acetylated and
303 non-acetylated pull-downs, we also detected an apicoplast localized acetyl-CoA carboxylase ACC1
304 (TGME49_221320) (Fig. 8 and Table S1). It is interesting to observe that an apicoplast protein displayed a
305 significant number of peptides, indicative of a consistent interaction which could occur if H2B.Z presents in
306 some situation an extracellular location as has been observed in other systems [53-57].

307

308

309 **Discussion**

310 In *T. gondii* gene expression is associated to the cell cycle, lytic cycle and differentiation [15, 58-63].
311 In addition to gene expression, the presence of histone variants as well as the turnover of PTMs on histones
312 are also associated to chromosomal organization, DNA repair or DNA replication [64]. The Apicomplexa
313 H2A.Z/H2B.Z double variant histone nucleosome is unique and is extensively modified by PTMs including N-
314 terminal tail acetylation. *T. gondii* epigenome has been studied, and it has been observed that this parasite
315 uses a set of different histone modifications as a complex set of tools to control its gene expression [65].
316 Acetylation and methylation are associated to opposite impacts in gene expression, the first favoring
317 expression, while the second is often a repressive mark. As an example, acetylation of lysine 31 on histone
318 H4 (H4K31) was associated to the promoter of a nearby active gene, while in the core body of these genes
319 H4K31me1 was detected [64]. Until now, the role of PTMs in *T. gondii* H2BZ has not been studied. However,
320 *T. gondii* H2B.Z/H2A.Z double variant nucleosomes were found in the promoter of active genes and in the

321 gene body of inactive genes [17]. This change in genomic location could be regulated by the different PTMs
322 of H2B.Z and/or H2A.Z. The present work is the first attempt to decipher the role of the N-terminal
323 acetylation of H2B.Z.

324 According to the results obtained in this work, the presence of a constitutive positive charge patch
325 in the N-terminal tail of the histone (c-Myc-R mutant) causes an increase in differentiation, a decrease in
326 growth, and an impaired DNA damage response *in vitro*. On the other hand, virulence was severely affected
327 *in vivo* indicating some sort of regulation at least in those processes for this H2B.Z PTM. Those effects were
328 not observed when lysine was replaced by alanine, an uncharged amino acid that mimics acetylated lysine,
329 except a mild effect on virulence *in vivo*. For *T. termophila* when engineering a constitutively positive charge
330 patch on H2A.Z, this was highly toxic, suggesting that its regulation has an essential function [66]. Moreover,
331 the presence of a single acetylation site in this region was sufficient to avoid the toxic effect of the positive
332 charge patch [66, 67]. In our case, some phenotypical alterations were observed *in vitro*, but the *T. gondii* c-
333 Myc-R tachyzoites were viable except during mouse infection. This indicates that at least *in vitro*, if there is a
334 toxicity due to the constitutive positive charge patch of H2B.Z, it could be partly compensated by H2A.Z,
335 which presents 10 acetylatable lysines [28]. Together, H2A.Z/H2B.Z, would represent a "combined N-terminal
336 tail" of 15 lysines. Studies involving the role of acetylation on H2A.Z N-terminal tail of *T. gondii* are needed
337 to understand this.

338 An interesting aspect is that the *T. gondii* c-Myc-R line can grow responding to DNA damage *in vitro*,
339 with significant but surmountable defect. This would indicate a role in DNA damage repair for this histone
340 variant in *T.gondii*, with acetylation as a central player. However, this sensitivity was only significant for c-
341 Myc-R tachyzoites, arguing once again in favor of the positive charge patch toxicity hypothesis in this mutant.
342 Since H2B.Z does not exist in nature beyond Apicomplexa, we can only infer the putative role of this variant
343 histone being part of H2A.Z/H2B.Z nucleosome. The participation of H2A.Z in DNA damage repair pathways
344 has been studied in mammals and yeast [20, 43, 44]. In those cases, H2A.Z was found to be involved in repair

345 due to genotoxic agents such as MMS and HU [44]. In our case, H2B.Z only demonstrated sensitivity with
346 MMS and not with topotecan, supporting the possibility that H2B.Z/H2A.Z work together in the same
347 function.

348 The contributions of effects observed *in vitro* are less difficult to ascertain in the *in vivo* model. Clearly
349 c-Myc-R line is capable of invasion, generating an adequate immune response, but it is quickly neutralized
350 during the infective process. This suggests that the tachyzoite is exposed *in vivo* to stronger environmental
351 pressures than those observed *in vitro*. These pressures would include adaptation to new environments,
352 including different cell types and organs, which may present differences in metabolism, nutrient availability,
353 or immune responses. Under these conditions, where the tachyzoite must respond quickly, fine
354 reprograming of gene expression and modifications in metabolic pathways would be required and the
355 impossibility of modulating the positive charge patch of H2B.Z could hamper the ability of parasites to adapt
356 to changing environments *in vivo*.

357 A possible explanation for the changes provoked by the positive charges in the N-tail could be a
358 chromatin compaction due to interaction with the negative charges in DNA. Genome size expansion in
359 eukaryote evolution has led to an increase in histone H2A N-terminal tail arginines. Arginine-rich histones
360 bind more tightly to DNA, compacting chromatin and, in some cases, the nuclei are also smaller [68].
361 However, in this work we showed that nuclei size was smaller in both clones compared to parental and to c-
362 Myc-WT-OE tachyzoites, indicating that the charges in the N-terminal tail are not responsible for chromatin
363 compaction. Chromatin compaction has also been described to be regulated by linker histone H1, that
364 stabilizes the nucleosome structure. A candidate H1 has been recently identified in *T. gondii*, and interaction
365 of H1 with H2B.Z was observed [69]. The acetylation status of H2B.Z may be important for this interaction,
366 leading to a more compact chromatin in both alanine and arginine mutants because of linker histone H1.
367 Further experiments are needed to test this hypothesis.

368 It could be expected that the phenotypic alterations are given by defects in the formation of the
369 nucleosome with an impact on the expression of the genes. In our analysis, both situations are not altered.
370 Although a massive analysis of gene expression is necessary to detect specific changes, part of the study
371 shows that the expression of Rop5 and Rop18 does not occur at the transcriptional level, but rather post-
372 transcriptionally, affecting their translation. This regulation could be given by the presence of non-coding
373 RNAs (ncRNAs) and there is increasing evidence for a significant role for pos-transcriptional mechanisms [70,
374 71]. Future studies should take this possibility into account, considering a possible role of H2B.Z acetylation,
375 to analyze ncRNAs expression in *T. gondii*. With the results shown in this work it is only possible to correlate
376 the decrease in one of the more virulent isoforms of Rop5 together with the absence of Rop18 protein to the
377 loss of virulence of c-Myc-R mutant, although it cannot be ruled out that other virulence factors could be
378 altered in these parasites. On the other hand, the absence of Rop18 protein in c-Myc-A correlates with the
379 significative delay in mice death with c-Myc-A tachyzoites infection as reported by Resse et al [49].

380 We could not detect significant changes in most of the genes analyzed by RT-qPCR in normal
381 conditions for tachyzoites, except for *BFD1* in c-Myc-R. This does not discard an association of the N-terminal
382 tail of H2B.Z with the epigenetic modulation of gene expression in some circumstances, for example in
383 changing environments, in an *in vivo* model. Regarding the significant expression of BFD1 mRNA, it is
384 intriguing if it is related to the high differentiation rate observed *in vitro* for these parasites. It is important
385 to note that the expression of the BFD1 gene is post-transcriptionally regulated [14]. Therefore, the increase
386 in transcription *per se* is not enough to induce differentiation, but the higher levels of BFD1 mRNA could favor
387 differentiation under alkaline stress. There is also another possibility of inducing differentiation based on
388 epigenetic regulation. HDACi FR235222 treatment was shown to favor acetylation of H4K31ac in bradyzoite
389 gene promoters, promoting transcription of bradyzoite genes and therefore, bradyzoite development [64].
390 Maybe under differentiation stress, H2B.Z is implicated in a fine regulation of gene expression through the

391 acetylation level of its N-terminal tail. Keeping that in mind, the lack of modulation of H2B.Z in c-Myc-R could
392 result in a different chromatin firing up the expression of bradyzoite-specific genes under alkaline stress.

393 Both acetylated and unacetylated peptides pull-downs share 3 nuclear proteins: GCN5A, PHD and
394 clathrin. GCN5A was shown to impact on H2A.Z acetylation via crosstalk with H4 acetylation by means of
395 bromodomain in p300 [72]. On the other hand, unacetylated peptide recognized one protein specifically, a
396 RNA recognition motif (RRM)-containing protein (TGME49_262620), which was also pulled down with GCN5b
397 acetyltransferase [60]. RRM-containing proteins are involved in post-transcriptional gene expression
398 processes, such as mRNA and rRNA processing, RNA export, translation, localization, stability, and turnover
399 [73]. In the case of acetylated peptide, it pulled down 2 specific proteins: a cyclin-dependent kinase regulator
400 (CDK_ TGME49_219832) and H3.3 histone variant (TGME49_218260). CDKs phosphorylate multiple
401 substrates that regulate the cell-division cycle in response to different cellular cues [74]. H3.3 and H2A.Z are
402 associated to promoter regions flanking the nucleosome depleted region (NDR) of active genes [75].
403 Therefore, it may be likely that acetylated H2A.Z and H2B.Z would associate to this variant histone in active
404 promoters. However, this association was not found in our genome wide analysis on tachyzoite stage [17].

405 In addition, CDKs have also been linked to mitosis [76, 77] and H3.3 is related to chromosome
406 segregation, nuclear structure, and the maintenance of genome integrity [78]. In this direction, it is
407 interesting that our pull-down assay has also retrieved, only for the acetylated peptide, other genes, all of
408 them associated to chromosome segregation (Table S1). Among them, peptidase c50 (TGME49_262825) a
409 separase or caspase-like protease, known to play a central role in the chromosome segregation [79].
410 Structural maintenance of chromosomes (SMC) proteins -like RecF/RecN/SMC N terminal domain-containing
411 protein (TGME49_231170)- function together with other proteins in a range of chromosomal transactions,
412 including chromosome condensation, sister-chromatid cohesion, recombination, DNA repair and epigenetic
413 silencing of gene expression [80-82]. Finally, meiotic recombination protein DMC1 family (TGME49_216400)
414 participate in meiotic recombination, specifically in homologous strand assimilation, which is required for the

415 resolution of meiotic double-strand breaks [83]. These findings open an interesting question, which could
416 implicate the role of H2A.Z/H2B.Z in the process of mitosis and chromosome segregation in the future.

417 It is relevant that these tachyzoites were able to generate a complete immune response, which only
418 happens when cells are invaded by tachyzoites and not with an infection with dead or lysed tachyzoites [84-
419 87]. In this sense, Toxovac® is a live attenuated vaccine used to prevent sheep congenital toxoplasmosis [88].
420 Recently, a Ca^{2+}-dependent protein kinase (CDPK) knock-out in Me49 type II strain was evaluated in mice as
421 a potential vaccine candidate [89]. The protection we observed in this work generated in mice facing an
422 infection with virulent RH tachyzoites is encouraging to continue with the proper assays needed for the
423 formulation of a vaccine.

424

425 Conclusion

426 In this work, we have shown that N-terminal tail lysine acetylation of histone H2B.Z is important for
427 the normal progression of *Toxoplasma gondii* life cycle. The presence of 5 positive charges in the N-terminal
428 of H2B.Z is most likely to be detrimental for the parasite. However, this toxicity is not very high, allowing the
429 parasite to replicate, but conferring a lower fitness to the tachyzoite. Moreover, this lower fitness is traduced
430 in a higher sensitivity to DNA damage, a mis-regulation of gene expression conducing to a higher
431 differentiation rate *in vitro*, and also a complete lack of virulence when facing the immune response in mice.
432 All these effects are not explained by an heterochromatinization of DNA due to the interaction with the
433 positive charges, because we observed that nuclei are also smaller in c-Myc-A tachyzoites. Besides, the
434 effects cannot be explained by a dislocalization of the histone in the genome because the nucleosome is still
435 constituted normally. However, it is quite unlikely to find a physiologically a situation where the histone
436 would be completely unacetylated, and c-Myc-A tachyzoites may reflect the normal condition observed *in*

437 *vivo*. Therefore, the similarity observed between c-Myc-A and parental tachyzoites in most experiments
438 performed in this work, would confirm that in normal conditions H2B.Z is acetylated in *T. gondii*.

439 The findings in this work are not exclusively explained by regulation of gene expression. This is not
440 surprising, as it is known that histone proteins may exert other functions, related for example to cell division.
441 Even extra-nuclear functions are attributed to histones in many models, and research in this area could bring
442 new insights for *T. gondii* as well. Deficiencies in *Trypanosoma cruzi* H2Bv histone variant amount present
443 similar phenotypes as observed here, and the authors also proposed a putative extra-nuclear or extra-
444 nucleosome function [57].

445 Having a better understanding of how chromatin, chromosome maintenance, DNA integrity, DNA
446 replication, and gene expression are modulated in *T. gondii* will allow inferring about chromatin modulation
447 in other parasites of the phylum as well as the possibility of suggesting a novel mechanism of epigenetic
448 regulation in organisms with complex life cycles that are evolutionarily distant from fungi and vertebrates.

449

450

451

452 # Materials and methods

453 **Parasite culture and manipulation**

454 RHΔ*hxgprt* strain was used in all cases and grown in standard tachyzoite conditions *in vitro*: hTERT (ATCC®
455 CRL-4001, USA) monolayers were infected with tachyzoites and incubated with Dulbecco's modified Eagle
456 medium (DMEM, Invitrogen) supplemented with 1% fetal bovine serum (FBS, Internegocios S.A.,

457 Argentina) and penicillin (10,000 units/ml)-streptomycin (10 mg/ml) solution (Gibco, Argentina) at 37°C and
458 5% CO_2.

459 **Cloning over-expression strategy**

460 To generate the c-Myc-H2B.Z WT construct, the open reading frame (ORF) was amplified using the primers
461 F: 5'-ATGCATTCAGGGAAAGGTCCGGCACAG-3' and R: 5'-TTAATTAACTATGCACCAGAAGTCGTG-3'. For the
462 mutant constructs, reverse primer was the same, and forward was:
463 ATGCATTCAGGG**GCA**GGTCCGGCACAG**GCA**TCTCAGGCGGCG**GCGGCG**ACCGCCGGG**GCG**TCTCTGGGAC for c-
464 Myc-A, ATGCATTCAGGG**CGC**GGTCCGGCACAG**CGC**TCTCAGGCGGCG**CGCCGC**ACCGCCGGG**CGC**TCTCTGGGAC
465 for c-Myc-R, where lysine coding codons were replaced for alanine and arginine coding codons, respectively
466 (in bold type). NsiI and PacI restriction sites (underlined) were engineered into the 5' end of primers F and R,
467 respectively, to clone into *T. gondii* expression vector PTUB8mycGFPPfTailTy-HX (a kind gift of Dr. Dominique
468 Soldati, Université de Geneve) with a strong tubulin promoter. The resulting PCR product of the expected
469 size was removed using a Qiaex II Gel Extraction kit (Qiagen), cloned in pGEM-T vector (Promega) and
470 sequenced (Macrogen). The cloned ORF was digested with NsiI and PacI and ligated into the plasmid. The
471 final plasmids were electroporated into RH strain tachyzoites lacking hypoxanthine–xanthine guanine
472 phosphoribosyl transferase (RH∆*hxgprt*). Transgenic parasites were selected in mycophenolic acid (25 μg/ml,
473 Sigma) and xanthine (50 μg/ml, Sigma) and cloned by limiting dilution.

474 **CRISPR/Cas9 gene deletion strategy**

475 Single guide RNAs were designed directed to the N-terminal portion of the *h2bz* gene: F:
476 AAGTTGAGGCGGCGAAGAAGACCGCCG and R: AAAACGGCGGTCTTCTTCGCCGCCTCA. Bsa I restriction sites
477 were included (underlined). Both oligos were annealed and cloned into the pU6 CRISPR Universal plasmid
478 (kindly provided by Lourido´s Lab, Whitehead Institute), by using the Bsa I restriction site. The plasmids were
479 confirmed by PCR, using the gRNA as primers, were sequenced (Macrogen) and prepared for transfection in

480 *Toxoplasma*. In order to obtain a clean KO, oligos were also designed to amplify the DHFR selection cassette
481 from the pUPRT_DHFR plasmid available in the laboratory, with homology regions (20 bp underlined) to the
482 3´and 5´UTR of the *h2bz* gene (F:
483 GAAAGGTCCGGCACAGAAATCTCAGGCGGCGAAGAAGACCAAGCTTCGCCAGGCTGTAAATCC, and R:
484 GAATTCCCTCTCAACATCAAATTTCACCCCGTGGTTTATTCCTCATCCTGCAAGTGCATAGAAGGA). The PCR
485 amplification product was purified from agarose gel and used to co-transfect the parasites along with the
486 CRISPR plasmid. c-Myc-R and c-Myc-A tachyzoites (one clone for each one was selected) were transfected
487 and Pyrimethamine (1 μm, Sigma) was used for selection. Cas9 was detected in the nucleus of the parasites
488 after transfection by using α-Flag antibody (Sigma, F1804). Selection was continued until three passages and
489 cloning by limiting dilution was performed. Positive clones were selected by PCR with primers designed for
490 that purpose: TgH2Bv-upUTR-F: GTTGTCATGCGCATTTGCATCAC; TgH2Bv-downUTR-R:
491 GTGTGCACGCGTTATAATGAGCAC; Val-TgH2Bv-R: CATGCTCTTCTTCGACACACCAG; DHFRCX-F:
492 GTGGCATTTCACACAGTCTCACCTC; DHFRCX-R: AGACGCAGACGCATACAACGTTAG.

493 **Immunofluorescence assay (IFA)**

494 Intracellular tachyzoites grown in cover slips were fixed using cold methanol 100% for 8 min, washed with
495 PBS and blocked with 1% BSA. Primary antibody αrH2B.Z (rabbit), αrSag1 (mouse), αrHSP90 (rabbit), αrROP5
496 (rabbit), αrROP18 (rabbit) produced in the laboratory and αc-Myc (rabbit, abCam ab9106 or mouse, Santa
497 Cruz sc-42), αAcTubulin (mouse, Millipore MABT868) were incubated for 1 h at room temperature. After
498 several washes with PBS cover slips were incubated with secondary antibodies Alexa fluor goat anti-mouse
499 488 and anti-rabbit 594 (Invitrogen). DAPI was used to stain nuclei. Axio Imager.M2 Microscope Carl Zeiss
500 (Germany) with objective Plan-Apochromat 63x/1.40 Oil M27 and Video digital camera Zeiss 503
501 monochromatic 2.8 megapixeles, was used. Image J 1.53q (Fiji) software was used to process images.

502 **Western blot analysis**

503 Tachyzoites were collected, filtered, counted and lysed by 6 cycles of rapid freezing/defreeze in hypotonic
504 buffer, and boiled with LB for 5 minutes. 0.5 to 1×10^7 parasites were loaded per well and resolved by 15%
505 SDS-PAGE. Proteins were transferred to PVDF membrane for 1h at 100V. Western blot was then performed
506 as described [90]. The primary antibodies: αrH2B.Z [22], αrH2A.Z [23], αrROP5 (rabbit) and αrROP18 (rabbit)
507 were used at 1/5000, whereas α-c-Myc (rabbit, abCam ab9106) was used at 1/2000 and αrSag1 [87] 1/200
508 for 1 h at room temperature. αH3ac (rabbit, Millipore, 06-599B) 1/200, was incubated overnight. Appropriate
509 secondary antibodies were used: phosphatase alkaline-conjugated goat anti-mouse or anti-rabbit (Sigma)
510 along with the NBT and BCIP (Promega) detection system.

511 **Phenotypical assays**

512 For growth/competition assays, coverslips seeded with Htert cells were infected with a mix of 50% parental
513 (RHΔ*hxgprt*) and 50% of each clone. 3 coverslips per clone were infected with 0,05 to 0,1 tachyzoite per cell,
514 incubated 10 minutes on ice, and 2 hours at 37°C in incubator for invasion. Slides were washed twice with
515 PBS to remove tachyzoites that did not enter the cells, and fresh DMEM supplemented with 1% SFB was
516 added. Slides were fixed at different times, up to 96 hours and IFA was performed with α-c-Myc and α-Sag1
517 antibodies to distinguish between parental and c-Myc positive vacuoles. Number of c-Myc positive and total
518 vacuoles in at least 100 vacuoles, randomly choosing different fields of each slide were counted. In the case
519 of competition assays with genotoxic drugs treatment, the experiment was modified as follows: 3 slides per
520 clone mixture were fixed after 24 h, to stablish the initial percentage of c-Myc positive vacuoles. At this time
521 point, media was changed in the rest of the slides for DMEM supplemented with DMSO or drugs at the
522 concentrations indicated. These slides were fixed after 96 h, and IFA was performed and counted as explained
523 before.

524 For *in vitro* differentiation assays, in a similar way using Htert confluent slides, media was changed by DMEM
525 HEPES pH 8.1, after invasion with 1 parasite every 10 cells, accompanied with deprivation of CO_2. Media was

526 changed every day, and differentiation rate was estimated after 96 h by using *Dolichos Biflorus* Lectin
527 conjugated to Fluorescein (DLB 1:200, FL-1031; Vector Laboratories) to stain the wall of the cysts in formation
528 and α-Sag1 antibody to stain the tachyzoites. In the case of collection of parasites for RNA extraction,
529 differentiation assay was performed in a similar way, but in t25 dishes. After 48 or 96 h parasites were forced
530 out of the cells by 23G, 25G and 27G syringe passages.

531 For *in vivo* survival, virulence and differentiation assays, C57BL/6 female mice were used. For the use of
532 animals, C.I.C.U.A.E-UNSAM 10/22 was approved. Mice were maintained in optimal conditions in the
533 biotherium, with controlled temperature and free access to sterilized water and food. Infection was carried
534 out intra-peritoneal in 10 mice per group with 100, 1000 or 10000 tachyzoites of parental lines or clones,
535 depending on the assay. PBS was injected as negative control in five mice per experiment. Deceases were
536 registered along 30-35 days in each experiment, and signs of illness were monitored daily. Two mice from
537 each group (except PBS) were sacrificed at day 5 (when RH infected mice have symptoms of illness), and
538 intraperitoneal fluids were collected in order to detect acute *Toxoplasma* infection. Blood samples were
539 taken at days 0, 14, 21 and 35 and sera was frozen for ELISA assays. After sacrifice, surviving mice brains were
540 processed for cyst observance by optical microscopy. Also, a sample was stained using DLB and checked by
541 fluorescence microscopy.

542 In every phenotypical assay, three independent experiments were performed. One representative
543 experiment is shown.

544 **RT-PCR and RT-qPCR**

545 Tachyzoites or parasites exposed to 48 or 96 h differentiation stress as explained before were conserved in
546 TriZol (Invitrogen) solution at -80°C until use. All experiments were performed in three independent
547 replicates. RNA extraction was performed according to the manufacturer's instructions and cDNA was
548 obtained by means of MMLV reverse transcriptase (Promega) using oligo dT with the protocol provided with

549 the enzyme. For RT-PCR, primers used were: SAG1: Fw: TGAGAACCCGTGGCAGGGTAA; Rv:
550 GCTTTTTGACTCGGCTGGAA; TUB: Fw: ATGTTCCGTGGTCGCATGT; Rv: TGGGAATCCACTCAACGAAGT; ACTIN:
551 Fw: GGGCGGTTTCATGACCTAAA; Rv: ACGTATGATGCGCGAGAAAA; ROP5: Fw:
552 CTAGCTAGCATGGCGACGAAGCTCG; Rv: CCCAAGCTTTCAAGCGACTGAGGGCGCA; ROP18: Fw:
553 CTAGCTAGCATGTTTTCGGTACAGCGGCCA; Rv: GCCAAGCTTTTATTCTGTGTGGAGATGTTC.

554 For RT-qPCR primers used were: SAG1: Fw: TGAGAACCCGTGGCAGGGTAA; Rv: GCTTTTTGACTCGGCTGGAA;
555 BAG1: Fw:CAACGGAGCCATCGTTATCAAAGG; Rv: TAGAACGCCGTTGTCCATTG; LDH2:
556 Fw: ACAATGGCCCAGGCATTCT; Rv: CAATAAACATATCGTGAAGCCCATA; AP2IX-9:
557 Fw: GGGCGTTCTCAGCGTTCACT; Rv: GGCGCGTCTCATCTGTTTCA; AP2IV-3:
558 Fw: GAGCCCATTGACCCCATGAA; Rv: GGCTTCGCTTCTTTCCGTGA; BFD1: Fw:
559 ATGTCGGGAACGATGGTTTA; Rv: TCTTCACGGCATTCTCTGTG; TUB:
560 Fw: ATGTTCCGTGGTCGCATGT; Rv: TGGGAATCCACTCAACGAAGT; ACTIN: Fw: GGGCGGTTTCATGACCTAAA; Rv:
561 ACGTATGATGCGCGAGAAAA.

562 The primers were first assayed for efficiency using a pooled cDNA in 1 to 0.001 dilutions, and the threshold
563 was defined for each set of primers. Melt curves were also obtained for each set. For each set of experiments,
564 SybrGreen master solution (Roche) was used and qPCR was run in StepOne Real time equipment (Applied
565 Biosystems). Actin and tubulin were used as housekeeping genes and data was normalized to those genes
566 by Infostat software. For the experiments in figure 3, all sets of data were relativized to tachyzoite
567 amplification. For experiment shown in figure 7, data from the different clones was relativized to the
568 parental.

569 **ELISA assay**

570 Blood samples were extracted from surviving mice at days 0 (Pi), 14, 21 and 35. Sera was frozen until
571 processing for ELISA. TLA (Toxoplasma lysate antigen, obtained from fresh RH tachyzoites) in buffer

572 Carbonate (7,13g/L NaHCO3 + 1,59 g/L Na2CO3 pH 9,5) was used to immobilize 96 well plaques (Nunc
573 Immuno™ MicroWell™ 96 well solid plates, Sigma), o.n. at 4°C. After bocking with 5% non-fat milk in PBS-T
574 they were incubated with sera diluted 1:100 in the same solution. Total IgG (IgGt) and subtypes (IgG1, IgG2a
575 and IgG2b) HRP-conjugated anti-mouse, made in rat, were used 1:5000. Tetramethyl-bencidine (TMB,
576 Invitrogen) was used to reveal, and plaques were read after 20 min reaction at 655 nm in a Synergy H1. Data
577 was analyzed in GraphPad Prism v7. Sera from mice inoculated with PBS (negative control) or infected with
578 Me49 (positive control) were assayed.

579 **Co-Immunoprecipitation (Co-IP)**

580 Approximately 5×10^8 RHΔ*hxgprt* tachyzoites were used for each immunoprecipitation. Tachyzoites were
581 treated with micrococcal endonuclease (MNase) in order to obtain mononucleosomes as described [23] and
582 Co-IP was performed as described in Dalmasso et al [23] with minor modifications. Protease inhibitor cocktail
583 (Sigma) was added in every step. Mononucleosomes were incubated with Agarose c-Myc beads (abCam,
584 ab1253) overnight at 4°C. Immunocomplexes were washed twice with washing buffer 1 (50 mM Tris, pH8,
585 200 mM NaCl and 0.05 % Igepal100), twice with washing buffer 2 (50 mM Tris, pH8, 300 mM NaCl and 0.05
586 % Igepal100), and twice with buffer TE (10 mM Tris, pH8, 1 mM EDTA); then resuspended in 60 µl of SDS-
587 PAGE loading buffer. Samples were boiled for 5 min and 20 µl were loaded per well in a 15% SDS-PAGE gel
588 for immunoblotting. The absence of contaminating proteins was corroborated by Western blot with murine
589 anti-SAG1antibody [87]. Quantification of the bands was done with Image J 1.53q (Fiji) software.

590 **Tachyzoites nuclei size assay**

591 Three slides with confluent hTert cells were infected as explained before with parental or c-Myc-A/c-Myc-
592 R/c-Myc-WT-OE clones and let replicate for 24 hours. Slides were fixed and IFA was performed as explained
593 before using αrH2B.Z to stain nuclei. Images were processed with Image J 1.53q (Fiji) software to measure
594 the size of the nuclei, by delimiting them with the appropriate tool in at least 50 vacuoles in fields randomly

595 chosen, for each slide and each independent experiment. Data was graphed and statistical analyzed with
596 GraphPad Prism 8 software.

597 **Peptide synthesis and characterization**

598 Peptides were synthesized by solid-phase multiple peptide system using tea-bags with Fmoc/tBu strategy
599 according Guzmán [91], briefly: Rink amide resin (0.55 meq/g) was used as solid support and Fmoc amino acids,
600 including acetylated lysine (Iris Biotech). Peptides were couplet to biotin for their detection The peptide cleavage
601 was performed with a solution of Trifluoracetic acid/triisopropylsilane/1.2-ethandithiol /water (92.5 /2.5
602 /2.5/2.5), washed with cold ether dried and lyophilized. Peptides were characterized by HPLC and electrospray
603 ionization mass spectrometry, and purified by C18 cartridges (United Chemical Technologies, Bristol, PA, USA)
604 before use.

605 Peptides used in the pull-down assays were: Un-acetylated: GPAQKSQAAKKTAGKSLGPRK(Biotin)

606 Acetylated: GPAQKSQAAK(Ac)K(Ac)TAGKSLGPR-K(Biotin)

607 **Pull-down assays**

608 Pull-down experiments were performed as detailed in Wysocka [52] after nuclear extraction with NE-PER
609 commercial kit following manufacturer´s instructions (Thermo Scientific #78833) and run in SDS-PAGE for a
610 short time in order to avoid separation. Protein gels were fixed by soaking for 3 hr in 30% methanol, 2%
611 phosphoric acid. Then the gel was washed with deionized water 3 times, 5 minutes each. After removing the
612 deionized water, the staining solution (0.5 g/L Coomasie blue brilliant R250, 18% methanol, 17% $(NH_4)2SO_4$,
613 2% phosphoric acid) was added until covering the gel. It was stained for 1 h in gentle shaking. Then the gel
614 was rinsed in deionized water 3 times for 5 minutes each. The background staining was removed with 30%
615 methanol. The gel was stored in deionized water until use. Each lane of the gel was cut into individual slices.
616 Each band was then cut into 1 mm^3 cube and further treated with three washes of 50 mM NH_4HCO_3 in 50%
617 CH_3CN with 10 min incubations. Each group of gel cubes was then dehydrated in CH_3CN for 10 min and dried
618 in a Speed Vac. Protein samples were reduced by dithiothreitol (DTT) and alkylated by iodoacetamide [92]. A

619 solution of 10 ng/µL trypsin in 50 mM NH_4HCO_3 was used to re-swell the gel pieces completely at 4°C for 30
620 min, followed by a 37°C digestion overnight. A small amount of 10% formic acid was then added to stop the
621 digestion. The sample was then centrifuged at 2,800 x g, and the supernatant was collected for LC-MS/MS.

622 **LC-MS/MS Analysis**

623 A fused silica microcapillary LC column (15-cm long x 75-µm inside diameter) packed with Halo C18 reversed-
624 phase resin (2.7 µm particle size, 90 nm pore size, MichromBioresources.) was used with EASY-nLC 1200
625 system (Thermo Fisher). The nanospray ESI was fitted onto the Thermo Q-Exactive plus mass spectrometer
626 (Thermo Electron, San Jose, CA) that was operated in a Higher-energy C-trap dissociation mode to obtain
627 both MS and tandem MS (MS/MS) spectra. Two µL of tryptic peptide samples were loaded onto the
628 microcapillary column and separated by applying a gradient of 3-40% acetonitrile in 0.1% formic acid at a
629 flow rate of 300 nL/min for 80 min. Mass spectrometry data were acquired in a data-dependent top-10
630 acquisition mode, which uses a full MS scan from m/z 350-1700 at 70,000 resolution (automatic gain control
631 [AGC] target, 1e6; maximum ion time [max IT], 100 ms; profile mode). Resolution for dd-MS2 spectra was set
632 to 17,500 (AGC target: 1e5) with a maximum ion injection time of 50 ms. The normalized collision energy
633 was 27 eV.

634 **Protein Identification**

635 Obtained MS spectra were searched against the *T. gondii* ToxoDB-42 _TgondiiME49 protein database using
636 Proteome Discoverer 2.2 (Thermo Electron, San Jose, CA). The search parameters permitted a 10 ppm
637 peptide MS tolerance and a 0.02 Da MS/MS tolerance. Carboxymethylation of cysteines was set as a fixed
638 modification, and oxidation of methionine as a dynamic modification. Up to two missed tryptic peptide
639 cleavages were considered. The proteins for which the False Discovery Rate was less than 1% at the peptide
640 level were included in the following analysis. The raw data of all mass spectra had been submitted to the
641 MassIVE (https://massive.ucsd.edu/; Project accession: MassIVE MSV000091226).

642

643 **Author Contributions**: L.V. participated in all the experiments, analyses and design of the study and wrote the
644 first draft; D.M. performed Crispr/Cas9 and some of the characterization experiments along with the pull-down
645 experiments with L.V. supervision; C.C. performed the DNA damage experiments and some of the transfections;
646 A.G. was involved in many of the experiments with technical support, and was in charge of RNA and cDNA
647 preparation; R.N. performed RT-PCR experiments and ELISAs with LV supervision; M.C.B. performed Co-IP
648 experiments with L.V. supervison; V.T. perfomed Rop5 and Rop18 antibodies and provided the respective
649 primers for RT-PCR; F.G. synthesized biotynilated peptides for pull down experiments; B.D. performed mass
650 spectrometry analysis; K.K. and W.J.S. participated in design of the study and manuscript final corrections; S.O.A.
651 designed the study and participated in its supervision. All authors have read and agreed to the published version
652 of the manuscript.

653 **Funding**: This work was supported by the Ministerio Nacional de Ciencia y Tecnología (MINCyT): PICT 2015 1288
654 (S.O.A.), PICT 2018 2434 (L.V.), Consejo Nacional de Investigaciones Científicas y Tecnológicas (CONICET): PIP
655 11220150100145CO and 11220210100572CO (S.O.A., L.V.) and by National Institute of Health: NIH-NIAID
656 1R01AI129807 (S.O.A.) and AI152583 (to W.J.S.).

657 **Institutional Review Board Statement**: Not applicable.

658 **Informed Consent Statement**: Not applicable.

659 **Data Availability Statement**: The data that support the findings of this study are available from the
660 corresponding author upon reasonable request.

661 **Acknowledgments**: L. Vanagas (Researcher), D. Muñoz (Fellow), C. Cristaldi (Fellow), D. Ganuza (Technician), V.
662 Turowski (Researcher), and S.O. Angel (Researcher) are members of CONICET. S.O. Angel (Full) and L. Vanagas
663 (Adjunct) are Professors at Universidad Nacional General de San Martin (UNSAM). The Vermont Biomedical
664 Research Network (VBRN) Proteomics Facility is supported through NIH grant P20GM103449 from the INBRE
665 Program of the National Institute of General Medical Science (BD).

666 **Conflicts of interest**: The authors declare that there are no conflict of interest.

667

668 **FIGURES**

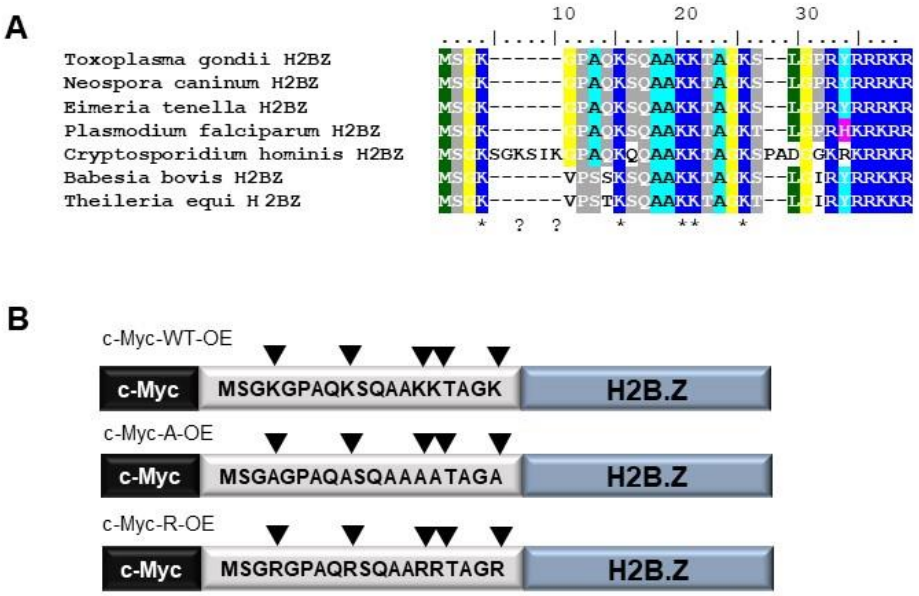

669

670 **Figure 1. H2B.Z N-terminal tail acetylation and mutagenesis strategy. A.** Representative Apicomplexa
671 H2B.Z N-terminal tail alignment. *Toxoplasma gondii* (TGME49_209910), *Neospora caninum*
672 (NCLIV_004160), *Eimeria tenella* (ETH_00030960), *Plasmodium falciparum* (PF3D7_0714000.1),
673 *Cryptosporidium hominis* (cgd7_1700-RA), *Babesia bovis* (BBOV_IV006840) and *Theileria equi*
674 (BEWA_028110) H2B.Z protein sequences were aligned by Clustal W. The N-terminal tail region is shown.
675 **B.** Scheme of the constructions generated in RHΔ*hxgprt* strain tachyzoites. The N-terminal region is shown
676 with the aminoacidic sequence, with or without mutations. All constructions were performed associated to
677 a tubulin promoter, in frame with a c-Myc tag in the N-terminal.

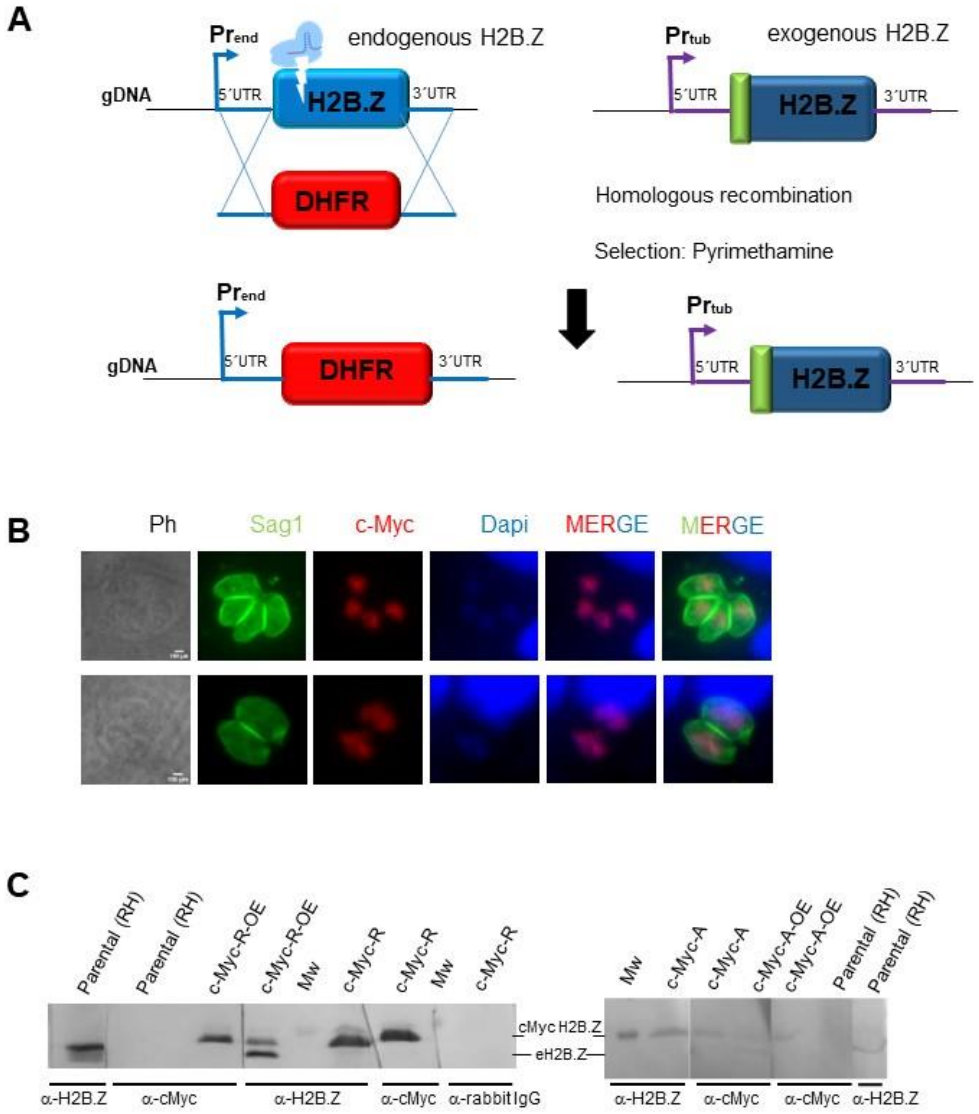

678

679 **Figure 2. H2B.Z gene deletion strategy**. **A.** CRISPR/Cas9 deletion of endogenous *h2b.z*, **s**trategy. Single guide
680 RNA was directed to the N-terminal region of H2B.Z. Tachyzoites of one clone c-Myc-R-OE and c-Myc-A-OE
681 were co-transfected with Crispr plasmid and a PCR product obtained with primers to amplify DHFR selection
682 cassette from pUPRT_DHFR plasmid with homology arms (20 pb) to 5´and 3´UTR of *h2b.z*. The scheme shows
683 the result of selection with Pyrimethamine and cloning, where parasites obtained replaced *h2b.z* by DHFR
684 cassette, and c-Myc-H2B.Z construction (with the corresponding mutations) remained. gDNA: genomic DNA;
685 Pr_{end}: endogenous promoter; Pr_{tub}: tubulin promoter. **B.** Immunofluorescence assay: coverslips seeded with

686 Htert cells at confluency were infected with 1 tachyzoite per cell of each obtained clone and fixed after 18-
687 24 hours. IFA was performed with α-cMyc (abCam), and α-Sag1 (mouse). α-IgG-mouse Alexa 488, and α-IgG
688 rabbit Alexa 564 were used 1:4000 for 30 minutes. DAPI was used to stain nuclei. Scale bar=5 μm. **C.** Western
689 blot assay. Clones confirmed by PCR were grown and lysed to run 0.5-1 x10^7 parasites per lane, transferred
690 to PVDF and assayed with indicated antibodies: α-c-Myc, α-H2B.Z, secondary α-rabbit IgG (negative control).
691 Over-expressing clones (c-Myc-R-OE and c-Myc-A-OE) used for transfection, as well as the parental (RH) were
692 loaded as controls. Mw: molecular weight marker (17 kDa band). eH2B.Z: endogenous H2B.Z.

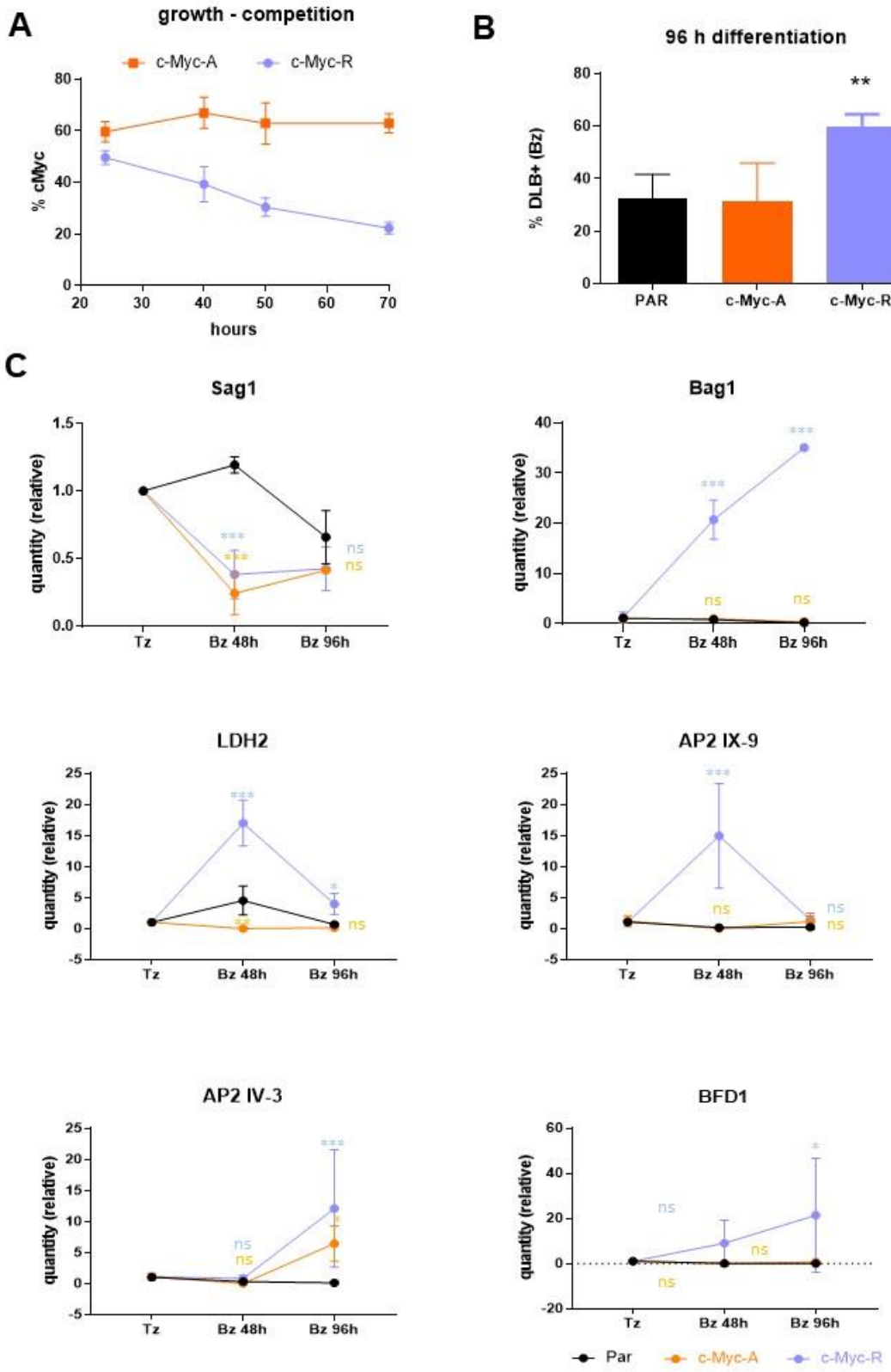
A
growth - competition
c-Myc-A
c-Myc-R
% cMyc
hours
B
96 h differentiation
% DLB+ (Bz)
PAR
c-Myc-A
c-Myc-R
C
Sag1
Bag1
LDH2
AP2 IX-9
AP2 IV-3
BFD1
quantity (relative)
Tz
Bz 48h
Bz 96h
Par
c-Myc-A
c-Myc-R

693

694 **Figure 3. *In vitro* growth and differentiation analysis on c-Myc-A and c-Myc-R**. **A.** Growth assay, performed
695 as explained in Materials and Methods. The percentage of c-Myc positive vacuoles is expressed as relative to
696 the total (α-Sag1), in at least 100 vacuoles per slide. Three slides per clone were counted. Representative
697 assay of three independent experiments. **B.** *In vitro* differentiation assay was performed as explained.
698 Percentage of DLB positive vacuoles was obtained after IFA with DLB and α-Sag1 to detect tachyzoites.
699 Representative assay of three independent experiments. PAR: parental (RHΔ*hxgprt)*. Data was analyzed with
700 Graphpad, and one-way Anova was performed. **: $p < 0.01$. **C.** Tachyzoites (Tz) of parental (RHΔ*hxgprt*); c-
701 Myc-A or c-Myc-R were freshly collected and conserved in Trizol until processing. *In-vitro* differentiation was
702 performed in dishes for 48 or 96 hours, and parasites were collected and conserved in Trizol. Every
703 experiment was performed in triplicate. RNA was extracted from each sample and cDNA was obtained by
704 reverse transcription with MMLV as explained in Materials and Methods. RT-qPCR was performed in Real
705 time PCR equipment (Applied Biosystems) with Sybr Green reagent with sets of primers indicated in each
706 graph, using tubulin and actin as housekeeping controls. Data was normalized to each of the housekeeping,
707 and relative quantities to tachyzoite in each sample is plotted for each of the genes studied. GraphPad Prism
708 was used to statisticaly analyze data, by two-way Anova. ***: $p < 0.0001$; **: $p < 0.01$; *: $p < 0.05$; ns: not
709 significant.

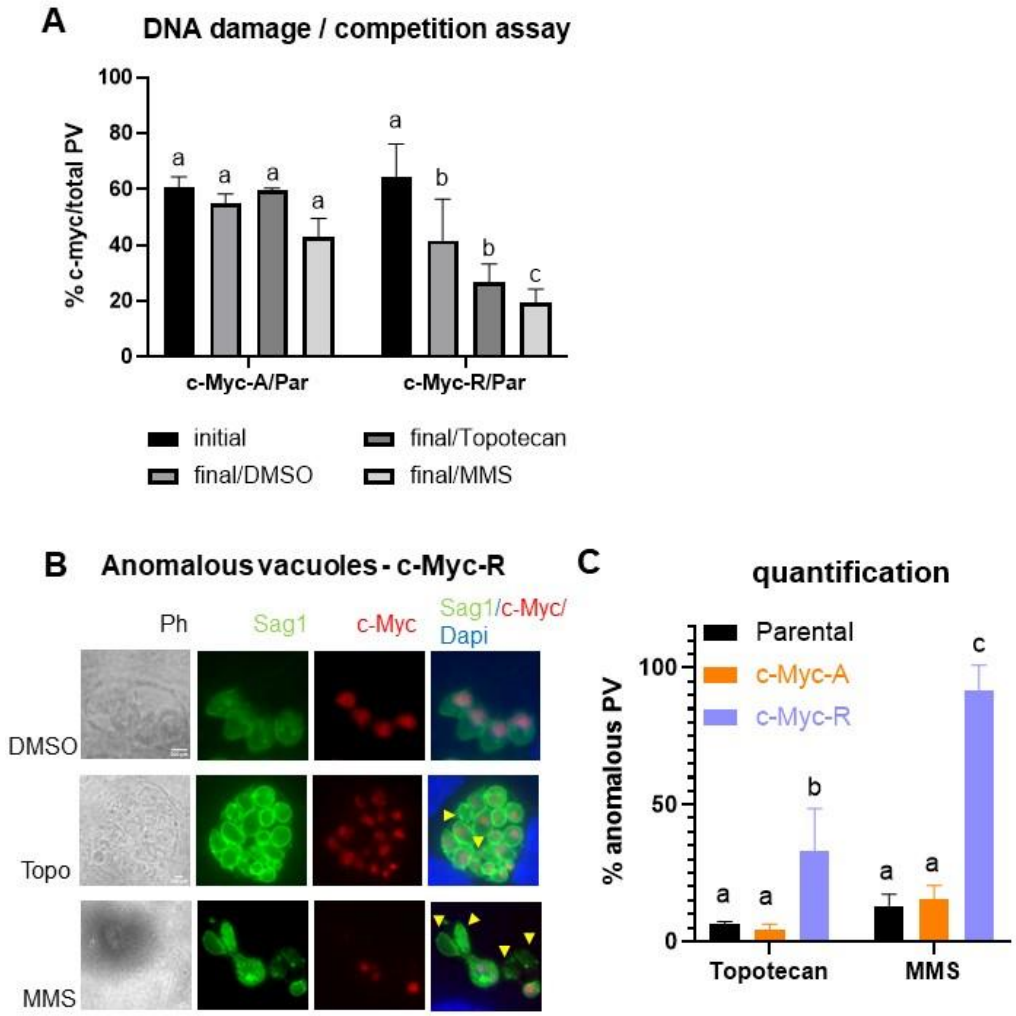

710

711 **Figure 4. H2B.Z acetylation status is important for DNA damage sensitivity. A.** Competition assay after DNA
712 damage induced by Topotecan (20 μM) or MMS (50 μM). Competition assay was performed as explained,
713 and IFA with anti-Sag1 for total vacuoles count and anti-cMyc for clones count was performed in three
714 independent experiments in triplicate. Graph shown corresponds to one representative assay. Initial: % of c-
715 Myc vacuoles of the total after 24 hours of infection with the mixture. Final: % of c-Myc vacuoles of the total
716 after 72 hours of treatment with each drug or DMSO as control. c-Myc-A/Par: mixture of c-Myc-A with
717 parental (RHΔ*hxgprt*) tachyzoites; c-Myc-R/Par: mixture of c-Myc-R with parental (RHΔ*hxgprt*) tachyzoites.
718 GraphPad Prism 8 statistical ANOVA analysis, multiple comparison where DMSO final is compared to initial
719 in each case and drugs data is compared to DMSO: a: ns; b: $p<0.05$; c: $p<0.01$. **B.** Vacuoles affected by drugs.

720 Representative images of most affected parasites (c-Myc-R) with both drug treatments. DMSO images are
721 included as control. Yellow arrowheads point to parasites with loss of genetic material. **C.** Quantification of
722 anomalous vacuoles. Anomalous and normal vacuoles were counted in at least 50 fields randomly chosen,
723 per clone, experiment and drug treatment. Results were plotted in GraphPad Prism 8 and statistical analysis
724 by Multiple comparisions was performed. a: ns; b: p<0.05; c: p<0.001.

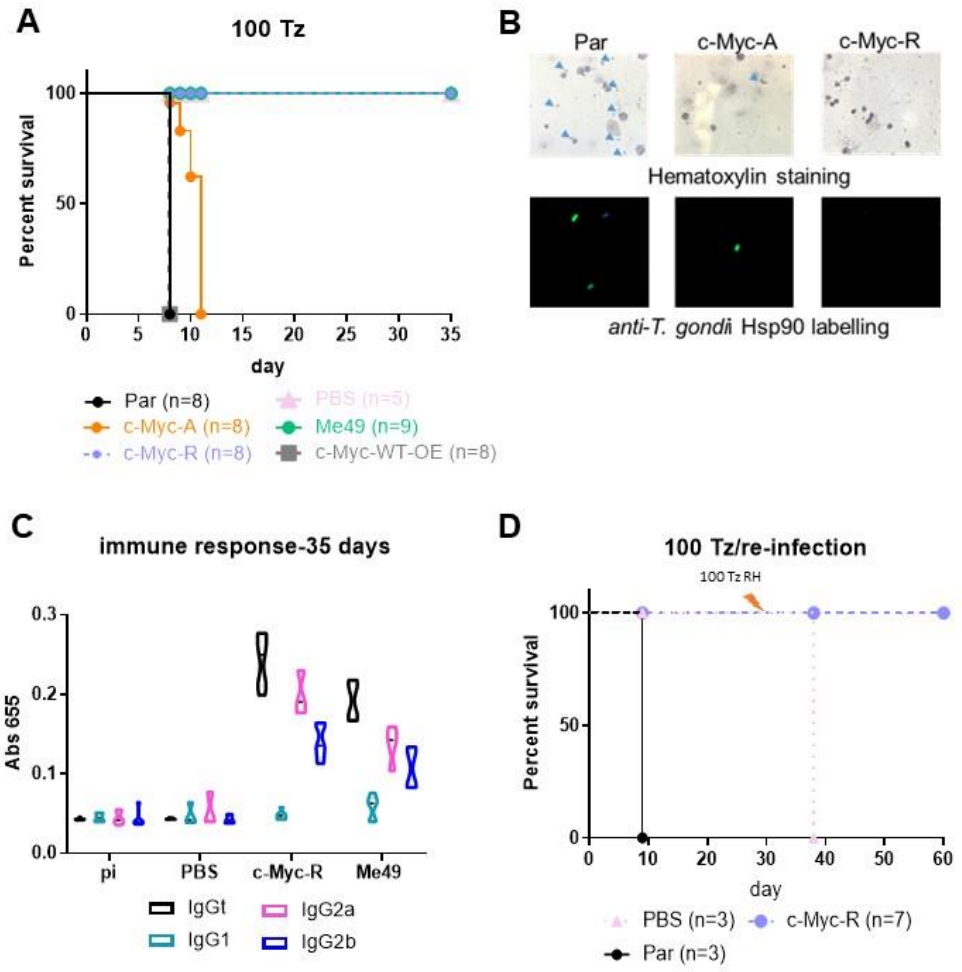

725

726 **Figure 5. c-Myc-R tachyzoites are not virulent i*n vivo* and elicit a protective immune response. A.** Survival
727 assay. 10 mice C57BL/6 were intra-peritoneal infected with either 100 tachyzoites of parental (RHΔ*hxgprt*),
728 and one clone of each KO line: c-Myc-R and c-Myc-A. As controls we also infected mice with c-Myc-WT-OE,
729 vehicle (PBS) and with Me49 tachyzoites (type II). The survival curve shown corresponds to one assay,

730 representative of three independent experiments. **B.** Acute infection. At day 5, 2 mice of each group were
731 sacrificed, and intra-peritoneal liquid was extracted and analyzed in the microscope, either by hematoxylin
732 staining (upper panel), or by IFA with α-HSP90 antibody (lower panel). Arrowheads in the upper panel show
733 tachyzoites. **C.** Evaluation of immune response by ELISA. Blood samples were extracted from surviving mice
734 at days 0 (Pi), 14, 21 and 35. Pooled sera from mice inoculated with PBS (negative control) or infected with
735 Me49 (positive control) were assayed. Total IgG and subtypes (IgG2a, IgG2b and IgG1) were analyzed. In the
736 graph only day 35 is shown. **D.** Re-infection assay. The indicated number of mice were infected with 1000
737 parental (Par) or c-Myc-R tachyzoites or inoculated with PBS. After 30 days, surviving mice were re-infected
738 with 100 parental RH tachyzoites. The survival curve shown corresponds to one assay, representative of three
739 independent experiments.

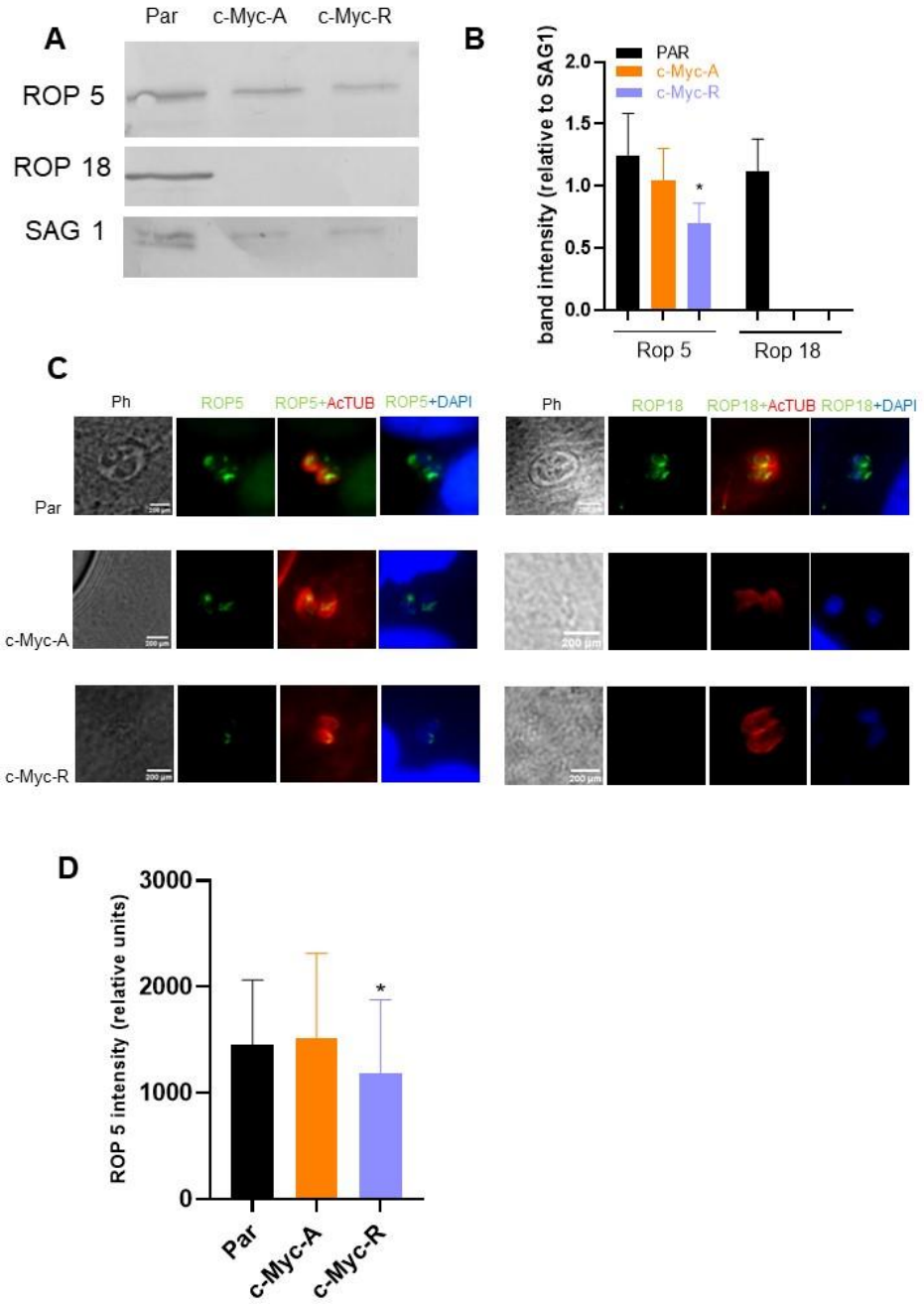

740

741 **Figure 6. Expression of ROP proteins is affected by H2B.Z acetylation. A.** Western blot identification of Rop5

742 and Rop18. The image is representative of three independent experiments, in which tachyzoite lysates of

743 parental (RHΔ*hxgprt*), c-Myc-A or c-Myc-R were run in SDS-PAGE, transferred to PVDF membranes and

744 assayed with anti Sag1 (charge control), anti Rop5 and anti-Rop18 antibodies. **B.** Quantification of band

745 intensities, relative to Sag1 band intensity in each lane. Image J software was employed to quantify relative
746 intensities and graphed with GraphPad Prism 8. Average plus SD of three independent assays is represented.
747 *: $p<0.05$. **C.** Immunofluorescence assay. Htert confluent slides were infected with tachyzoites of parental
748 (RHΔ*hxgprt*), c-Myc-A and c-Myc-R and fixed after 24 h for immunofluorescence analysis using anti Rop5 and
749 anti Rop18 antibodies (green). AcTubulin in red, was used to stain parasites and DAPI for the nuclei. **D.** Rop5
750 intensity quantification. Image J software was used to quantify the antibodies intensities in three
751 independent experiments, by triplicate, at least 10 vacuoles per slide. The graph shows the average intensity
752 in relative units; statistical analysis was performed by GraphPad Prism 8 software. *: $p<0.05$.

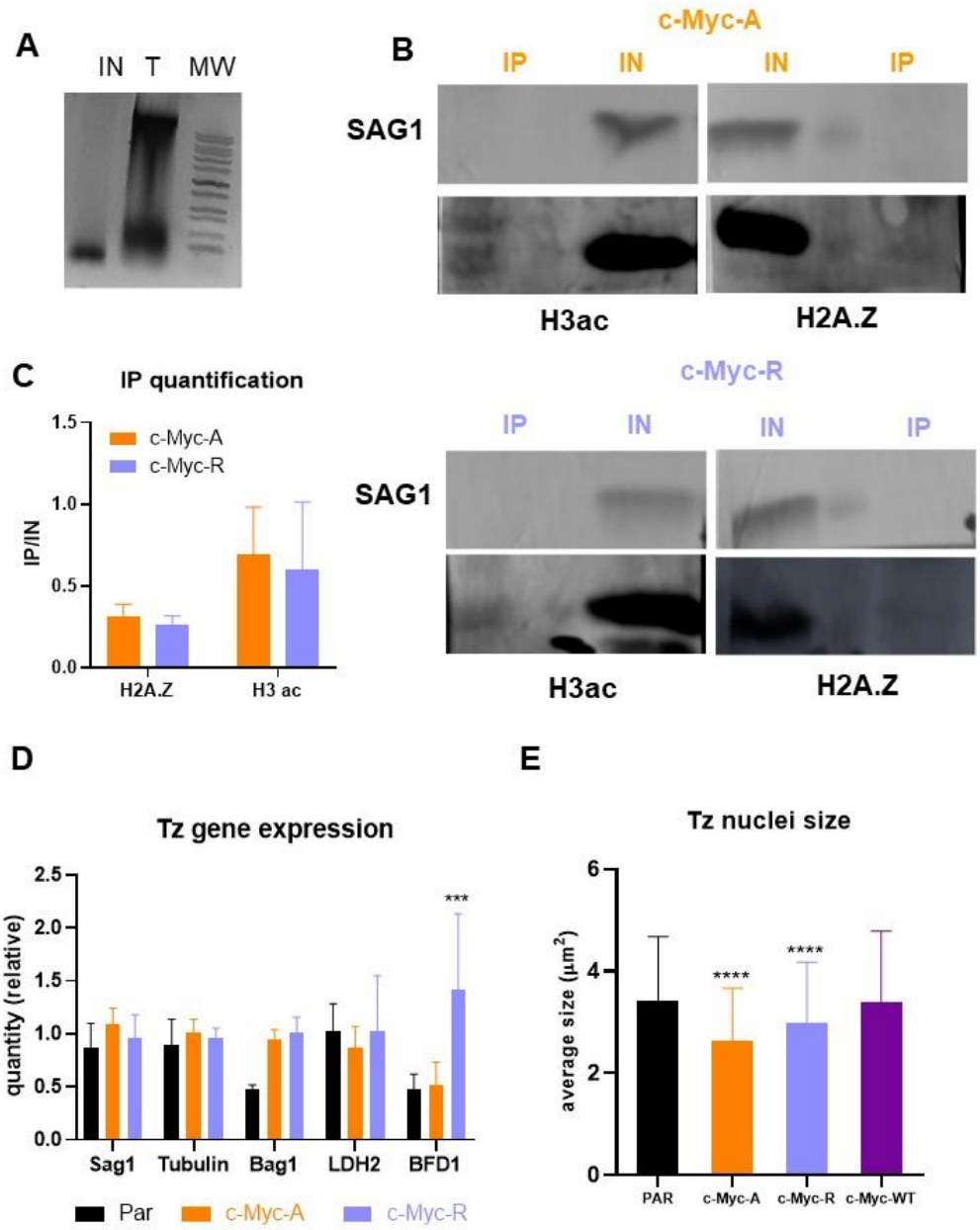

753

754 **Figure 7. Nucleosome composition and chromatin structure is maintained in c-Myc-A and c-Myc-R. A.**
755 Mnase digestion of tachyzoites for co-immunoprecipitation analysis. Tachyzoites were MNase digested as
756 explained in Materials and Methods, and an aliquot of the total tachyzoites and the digestion was
757 precipitated and run in 1% agarose gel. A representative image of digestion is shown. **B.** Co-
758 immunoprecipitation-WB analysis. Assays were performed in triplicate as explained in Materials and

759 Methods. A representative image of Western-blot analysis is shown for c-Myc-A and c-Myc-R. IP:
760 immunoprecipitation; IN: input. H3ac: western blot revealed with commercial anti H3acetylated antibody.
761 H2A.Z: western blot revealed with anti H2A.Z antibody performed in the lab. Sag1: western blot revealed
762 with anti Sag1 antibody. Color key: Orange for c-Myc-A; lilac for c-Myc-R. **C.** Quantification of western blot
763 band intensities. Image J software was used to quantify intensities of H3ac and H2A.Z IP bands and relativize
764 to respective IN band intensities. Graph shows the relative intensities of three independent experiments as
765 the average plus SD for each antibody and clone, with the same key color as before. Graphpad Prism 8
766 statistical analysis showed no significant differences between clones for both H3ac and H2A.Z quantification.
767 **D.** Tachyzoites gene expression. Tachyzoites (Tz) of parental (RHΔ*hxgprt*); c-Myc-A or c-Myc-R were freshly
768 collected in triplicate and conserved in TriZol until processing. RNA was extracted from each sample and
769 cDNA was obtained by reverse transcription with MMLV as explained in Materials and Methods. RT-qPCR
770 was performed in Real time PCR equipment (Applied Biosystems) with Sybr Green reagent with sets of
771 primers indicated in the graph, using actin as housekeeping control. Data was normalized to actin, and
772 relative quantities to RH tachyzoites in each sample is plotted for each of the genes studied. GraphPad Prism
773 was used to statistically analyze data, by two-way Anova. ***: $p< 0.0001$; ns: not significant. **E.** Tachyzoite
774 nuclei size. Tachyzoites of parental (RHΔ*hxgprt*), c-Myc-A, c-Myc-R or c-Myc-WT-OE were allowed to invade
775 hTert confluent slides and replicate for 20 h, and IFA was performed with α-H2B.Z antibody to detect the
776 nuclei. Image J software was used to measure the average nuclei size of at least 100 tachyzoites per slide, in
777 three independent experiments, and this was plotted and analyzed with Graphpad Prism 8, by two-way
778 ANOVA. ****: $p< 0.0001$.

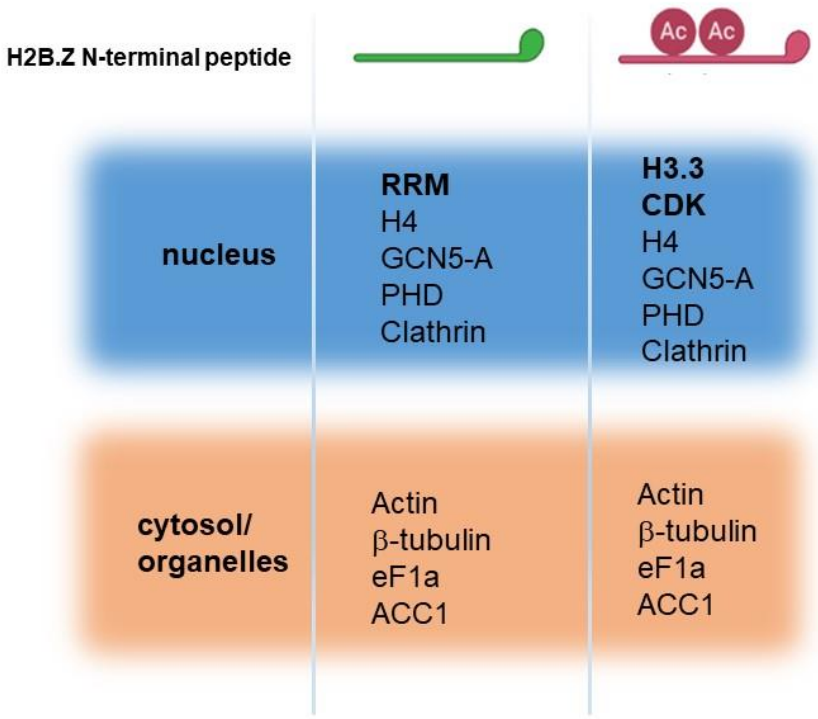

Figure 8. Identification of H2B.Z interacting proteins by pull-down assay. Scheme of the two different peptides synthesized is graphed above. Ac: acetylation. Most representative peptides retrieved in two independent assays for each peptide. Proteins are separated according to localization in nucleus or cytosol/organelles.

Supplementary figures

Figure S1

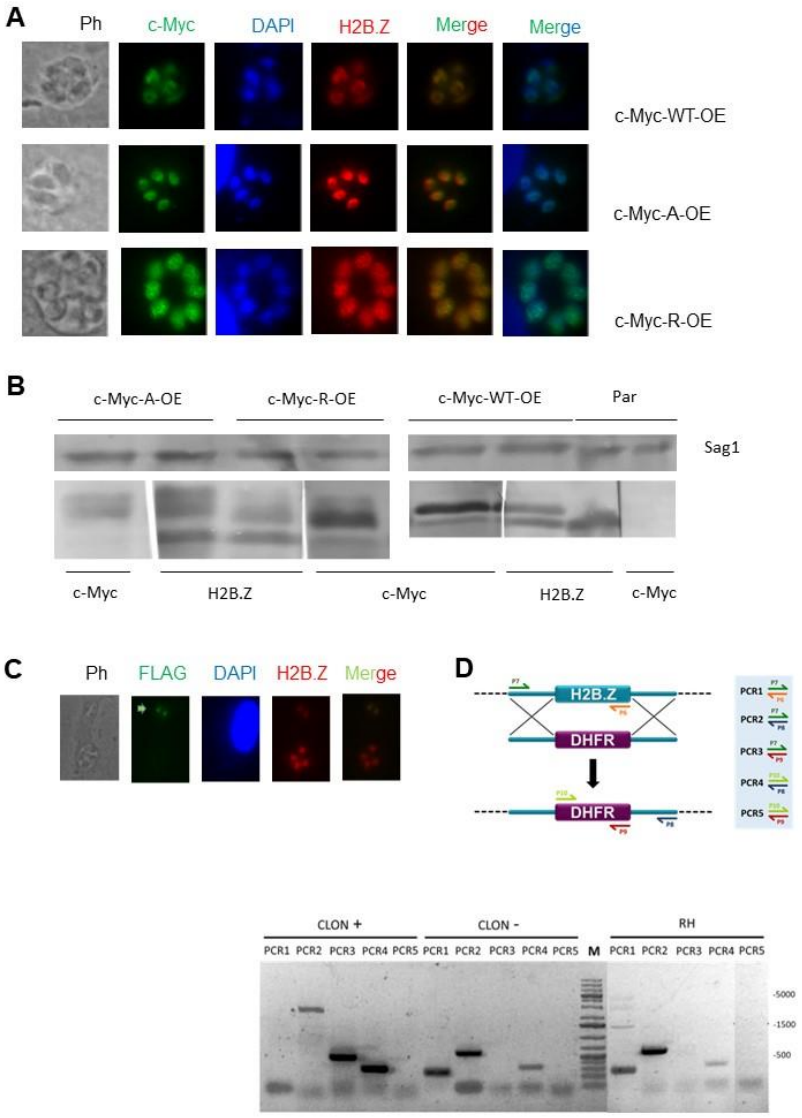

Fig. S1. Controls for tachyzoite lines over-expressing H2B.Z WT or mutants and CRISPR/Cas9 deletion of endogenous H2B.Z gene. A. Immunofluorescence assay. Htert confluent slides were infected with the different clones obtained and immunofluorescence was performed with anti c-Myc (green) and anti-H2B.Z (red); DAPI was used to stain nuclei. Images show a representative IFA of one clone of each over-expressing line obtained. **B.** Western-blot assay. One clone of each line and the parental were lysed and run in SDS-PAGE for WB assay with anti-H2B.Z, anti-c-Myc and anti-Sag1 (charge control). **C.** Immunofluorescence after transfection showing flag-CAS9 signal in the nucleus of one vacuole (green arrow). **D.** PCR selection of positive

795 clones. The scheme shows the primers designed for PCR detection of positive and negative clones. The image
796 corresponds to a representative PCR where a positive and a negative clone with the parental as control are
797 shown. PCR1-5: primers combinations for PCR shown in the scheme.

798

799 **Figure S2**

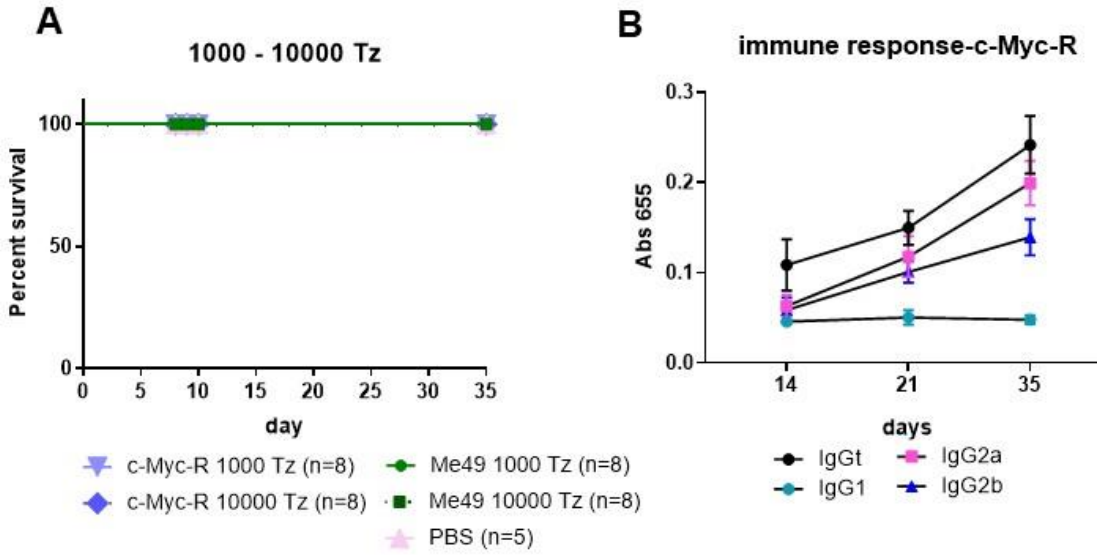

800

801 **Fig. S2. c-Myc-R tachyzoites up to 10,000 are unable to kill mice but immune response is triggered. A.**
802 Survival assay. 10 mice C57BL/6 were intra-peritoneal infected with either 1000 or 10000 tachyzoites of Me49
803 or c-Myc-R tachyzoites. Vehicle (PBS) was inoculated in 5 mice as control. The survival curve shown
804 corresponds to one assay, representative of three independent experiments. **B.** Evaluation of immune
805 response by ELISA. Assay shown in Fig. 5C, now showing data for 14, 21 and 35 days samples from mice
806 infeceted with c-Myc-R tachyzoites. Total IgG and subtypes (IgG2a, IgG2b and IgG1) were analyzed.

807

808 **Figure S3**

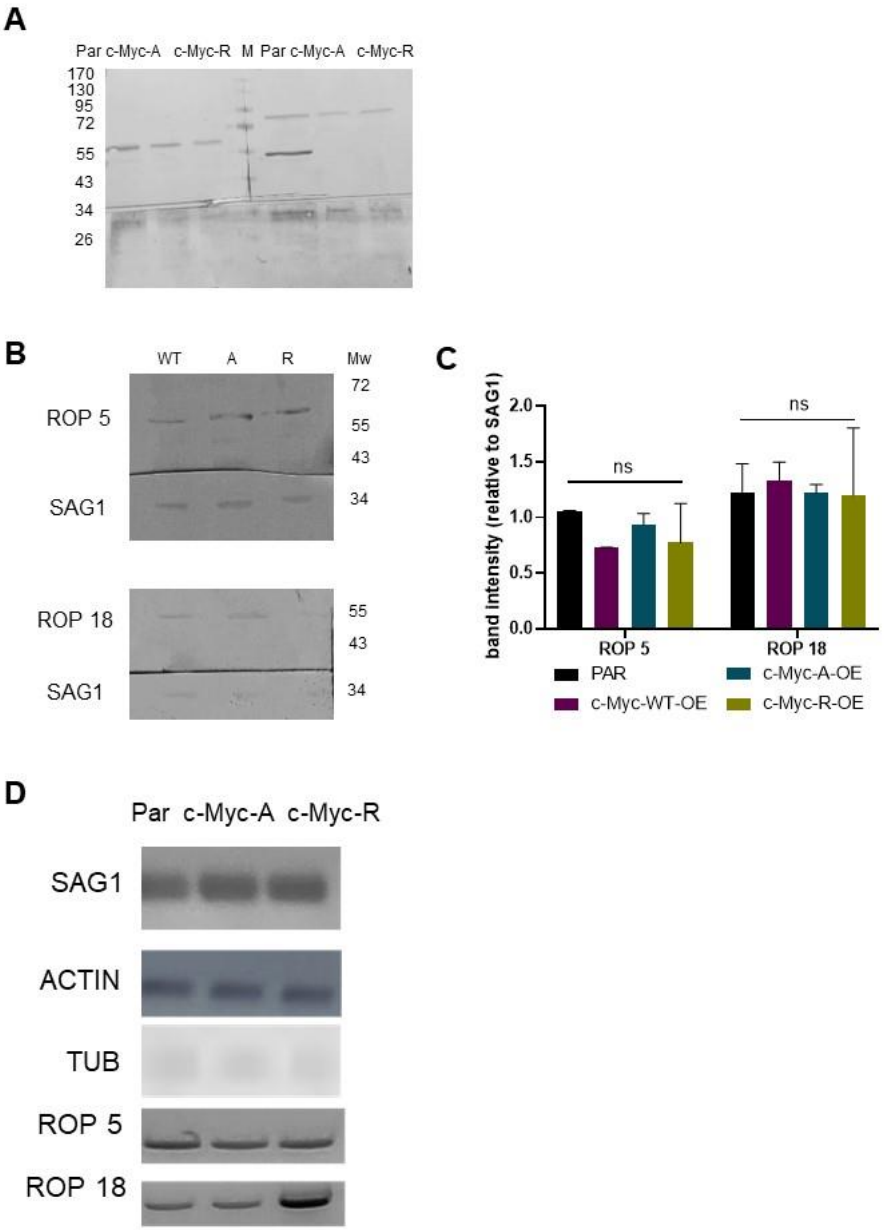

809

810 **Fig. S3. Western blot analysis of ROP proteins. A.** Complete image of Western blot shown in Fig. 5. **B.**
811 Representative Western-blot of over-expressing lines. Antibodies against Rop5, Rop18 and Sag1 were used.
812 WT: c-Myc-WT-OE; A: c-Myc-A-OE; R: c-Myc-R-OE. The upper bands detected with αRop18 are of higher
813 molecular weight than Rop18 full length protein, being unspecific. However, the intensities are similar to
814 Sag1, being a second charge control. **C.** Quantification of Rop5 and Rop18 bands, relativized to Sag1 band
815 intensity in each lane, in two independent WB experiments with the OE lines, and statistical analysis by

816 GraphPad Prism 8. ns: not significant. **D.** RT-PCR. Tachyzoites of parental (RHΔ*hxgprt*), c-Myc-A and c-Myc-R

817 were collected by triplicate and conserved in TriZol until RNA extraction, and cDNA preparation. PCR was run

818 with primers for the genes indicated and ran in agarose gels. Image is representative of three independent

819 experiments.

820

821 **Figure S4**

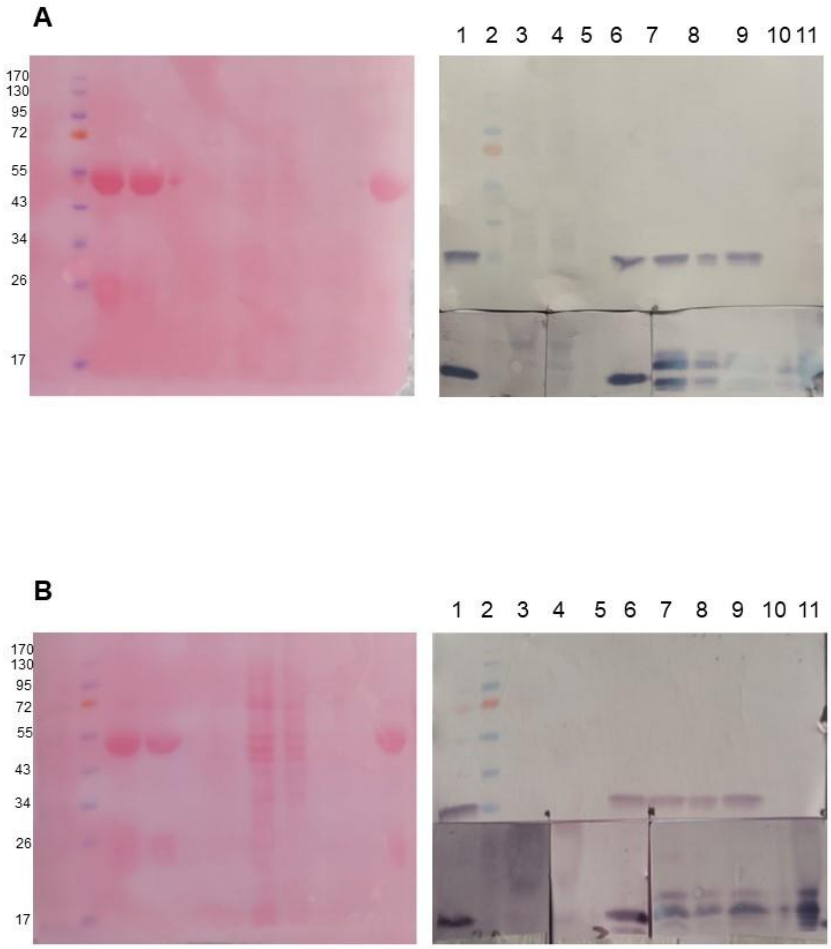

822

823 **Fig. S4. Co-immunoprecipitation assay. A.** Complete image of the Pounceau (left) and WB (right) shown in

824 Fig. 7 for c-Myc-A. **B.** Complete image of the Pounceau (left) and WB (right) shown in Fig. 7 for c-Myc-R. For

825 both images in lanes 1-11 was run: IN-M-IP-IP-space-IN-IN-T-NU-space-IP. IN: input; IP: immunoprecipitation;

826 T: total; NU: after immunoprecipitation, not bound to agarose beads. MW markers are indicated at the left.

827

828 # References

829 [1] Vanagas L, Jeffers V, Bogado SS, Dalmasso MC, Sullivan WJ, Jr., Angel SO. Toxoplasma histone
830 acetylation remodelers as novel drug targets. Expert review of anti-infective therapy. 2012;10:1189-
831 201.
832 [2] Mouveaux T, Rotili D, Boissavy T, Roger E, Pierrot C, Mai A, et al. A potent HDAC inhibitor blocks
833 Toxoplasma gondii tachyzoite growth and profoundly disrupts parasite gene expression. Int J
834 Antimicrob Agents. 2022;59:106526.
835 [3] Kim K. The Epigenome, Cell Cycle, and Development in Toxoplasma. Annual review of
836 microbiology. 2018;72:479-99.
837 [4] Pappas G, Roussos N, Falagas ME. Toxoplasmosis snapshots: global status of Toxoplasma gondii
838 seroprevalence and implications for pregnancy and congenital toxoplasmosis. Int J Parasitol.
839 2009;39:1385-94.
840 [5] Attias M, Teixeira DE, Benchimol M, Vommaro RC, Crepaldi PH, De Souza W. The life-cycle of
841 Toxoplasma gondii reviewed using animations. Parasit Vectors. 2020;13:588.
842 [6] Weiss LM, Kim K. The development and biology of bradyzoites of Toxoplasma gondii. Front Biosci.
843 2000;5:D391-405.
844 [7] Luft BJ, Remington JS. Toxoplasmic encephalitis in AIDS. Clin Infect Dis. 1992;15:211-22.
845 [8] Carlier Y, Truyens C, Deloron P, Peyron F. Congenital parasitic infections: a review. Acta Trop.
846 2012;121:55-70.
847 [9] Brynska A, Tomaszewicz-Libudzic E, Wolanczyk T. Obsessive-compulsive disorder and acquired
848 toxoplasmosis in two children. Eur Child Adolesc Psychiatry. 2001;10:200-4.
849 [10] Miman O, Mutlu EA, Ozcan O, Atambay M, Karlidag R, Unal S. Is there any role of Toxoplasma
850 gondii in the etiology of obsessive-compulsive disorder? Psychiatry Res. 2010;177:263-5.
851 [11] Yolken RH, Dickerson FB, Fuller Torrey E. Toxoplasma and schizophrenia. Parasite Immunol.
852 2009;31:706-15.
853 [12] Vittecoq M, Elguero E, Lafferty KD, Roche B, Brodeur J, Gauthier-Clerc M, et al. Brain cancer
854 mortality rates increase with Toxoplasma gondii seroprevalence in France. Infect Genet Evol.
855 2012;12:496-8.
856 [13] de Haan L, Sutterland AL, Schotborgh JV, Schirmbeck F, de Haan L. Association of Toxoplasma
857 gondii Seropositivity With Cognitive Function in Healthy People: A Systematic Review and Meta-
858 analysis. JAMA Psychiatry. 2021;78:1103-12.
859 [14] Waldman BS, Schwarz D, Wadsworth MH, 2nd, Saeij JP, Shalek AK, Lourido S. Identification of
860 a Master Regulator of Differentiation in Toxoplasma. Cell. 2020;180:359-72 e16.
861 [15] Jeffers V, Tampaki Z, Kim K, Sullivan WJ, Jr. A latent ability to persist: differentiation in
862 Toxoplasma gondii. Cellular and molecular life sciences : CMLS. 2018;75:2355-73.

863 [16] Bougdour A, Maubon D, Baldacci P, Ortet P, Bastien O, Bouillon A, et al. Drug inhibition of
864 HDAC3 and epigenetic control of differentiation in Apicomplexa parasites. The Journal of
865 experimental medicine. 2009;206:953-66.
866 [17] Nardelli SC, Silmon de Monerri NC, Vanagas L, Wang X, Tampaki Z, Sullivan WJ, Jr., et al.
867 Genome-wide localization of histone variants in Toxoplasma gondii implicates variant exchange in
868 stage-specific gene expression. BMC genomics. 2022;23:128.
869 [18] Santisteban MS, Kalashnikova T, Smith MM. Histone H2A.Z regulats transcription and is partially
870 redundant with nucleosome remodeling complexes. Cell. 2000;103:411-22.
871 [19] Oberdoerffer P, Miller KM. Histone H2A variants: Diversifying chromatin to ensure genome
872 integrity. Semin Cell Dev Biol. 2022.
873 [20] Xu Y, Ayrapetov MK, Xu C, Gursoy-Yuzugullu O, Hu Y, Price BD. Histone H2A.Z controls a critical
874 chromatin remodeling step required for DNA double-strand break repair. Mol Cell. 2012;48:723-33.
875 [21] Fenoy IM, Bogado SS, Contreras SM, Gottifredi V, Angel SO. The Knowns Unknowns: Exploring
876 the Homologous Recombination Repair Pathway in Toxoplasma gondii. Front Microbiol. 2016;7:627.
877 [22] Dalmasso MC, Echeverria PC, Zappia MP, Hellman U, Dubremetz JF, Angel SO. Toxoplasma
878 gondii has two lineages of histones 2b (H2B) with different expression profiles. Molecular and
879 biochemical parasitology. 2006;148:103-7.
880 [23] Dalmasso MC, Onyango DO, Naguleswaran A, Sullivan WJ, Jr., Angel SO. Toxoplasma H2A
881 variants reveal novel insights into nucleosome composition and functions for this histone family. J
882 Mol Biol. 2009;392:33-47.
883 [24] Dalmasso MC, Sullivan WJ, Jr., Angel SO. Canonical and variant histones of protozoan parasites.
884 Frontiers in bioscience. 2011;16:2086-105.
885 [25] Petter M, Selvarajah SA, Lee CC, Chin WH, Gupta AP, Bozdech Z, et al. H2A.Z and H2B.Z double-
886 variant nucleosomes define intergenic regions and dynamically occupy var gene promoters in the
887 malaria parasite Plasmodium falciparum. Molecular microbiology. 2013;87:1167-82.
888 [26] Lowell JE, Kaiser F, Janzen CJ, Cross GA. Histone H2AZ dimerizes with a novel variant H2B and is
889 enriched at repetitive DNA in Trypanosoma brucei. J Cell Sci. 2005;118:5721-30.
890 [27] Sidik SM, Huet D, Ganesan SM, Huynh MH, Wang T, Nasamu AS, et al. A Genome-wide CRISPR
891 Screen in Toxoplasma Identifies Essential Apicomplexan Genes. Cell. 2016;166:1423-35 e12.
892 [28] Nardelli SC, Che FY, Silmon de Monerri NC, Xiao H, Nieves E, Madrid-Aliste C, et al. The histone
893 code of Toxoplasma gondii comprises conserved and unique posttranslational modifications. mBio.
894 2013;4:e00922-13.
895 [29] Giaimo BD, Ferrante F, Herchenrother A, Hake SB, Borggrefe T. The histone variant H2A.Z in
896 gene regulation. Epigenetics & chromatin. 2019;12:37.
897 [30] Talbert PB, Henikoff S. Histone variants--ancient wrap artists of the epigenome. Nature reviews
898 Molecular cell biology. 2010;11:264-75.
899 [31] Bruce K, Myers FA, Mantouvalou E, Lefevre P, Greaves I, Bonifer C, et al. The replacement
900 histone H2A.Z in a hyperacetylated form is a feature of active genes in the chicken. Nucleic Acids
901 Res. 2005;33:5633-9.
902 [32] Binda O, Sevilla A, LeRoy G, Lemischka IR, Garcia BA, Richard S. SETD6 monomethylates H2AZ
903 on lysine 7 and is required for the maintenance of embryonic stem cell self-renewal. Epigenetics.
904 2013;8:177-83.
905 [33] Law C, Cheung P. Expression of Non-acetylatable H2A.Z in Myoblast Cells Blocks Myoblast
906 Differentiation through Disruption of MyoD Expression. J Biol Chem. 2015;290:13234-49.
907 [34] Valdes-Mora F, Song JZ, Statham AL, Strbenac D, Robinson MD, Nair SS, et al. Acetylation of
908 H2A.Z is a key epigenetic modification associated with gene deregulation and epigenetic remodeling
909 in cancer. Genome research. 2012;22:307-21.

910 [35] Whittle CM, McClinic KN, Ercan S, Zhang X, Green RD, Kelly WG, et al. The genomic distribution
911 and function of histone variant HTZ-1 during C. elegans embryogenesis. PLoS Genet.
912 2008;4:e1000187.
913 [36] Updike DL, Mango SE. Temporal regulation of foregut development by HTZ-1/H2A.Z and PHA-
914 4/FoxA. PLoS Genet. 2006;2:e161.
915 [37] Ridgway P, Brown KD, Rangasamy D, Svensson U, Tremethick DJ. Unique residues on the H2A.Z
916 containing nucleosome surface are important for Xenopus laevis development. J Biol Chem.
917 2004;279:43815-20.
918 [38] Myers FA, Chong W, Evans DR, Thorne AW, Crane-Robinson C. Acetylation of histone H2B
919 mirrors that of H4 and H3 at the chicken beta-globin locus but not at housekeeping genes. J Biol
920 Chem. 2003;278:36315-22.
921 [39] Miao J, Fan Q, Cui L, Li J, Li J, Cui L. The malaria parasite Plasmodium falciparum histones:
922 organization, expression, and acetylation. Gene. 2006;369:53-65.
923 [40] Trelle MB, Salcedo-Amaya AM, Cohen AM, Stunnenberg HG, Jensen ON. Global histone analysis
924 by mass spectrometry reveals a high content of acetylated lysine residues in the malaria parasite
925 Plasmodium falciparum. Journal of proteome research. 2009;8:3439-50.
926 [41] Radke JB, Lucas O, De Silva EK, Ma Y, Sullivan WJ, Jr., Weiss LM, et al. ApiAP2 transcription factor
927 restricts development of the Toxoplasma tissue cyst. Proc Natl Acad Sci U S A. 2013;110:6871-6.
928 [42] Hong DP, Radke JB, White MW. Opposing Transcriptional Mechanisms Regulate Toxoplasma
929 Development. mSphere. 2017;2.
930 [43] Gursoy-Yuzugullu O, Ayrapetov MK, Price BD. Histone chaperone Anp32e removes H2A.Z from
931 DNA double-strand breaks and promotes nucleosome reorganization and DNA repair. Proc Natl
932 Acad Sci U S A. 2015;112:7507-12.
933 [44] Morillo-Huesca M, Clemente-Ruiz M, Andujar E, Prado F. The SWR1 histone replacement
934 complex causes genetic instability and genome-wide transcription misregulation in the absence of
935 H2A.Z. PloS one. 2010;5:e12143.
936 [45] Munera Lopez J, Ganuza A, Bogado SS, Munoz D, Ruiz DM, Sullivan WJ, Jr., et al. Evaluation of
937 ATM Kinase Inhibitor KU-55933 as Potential Anti-Toxoplasma gondii Agent. Frontiers in cellular and
938 infection microbiology. 2019;9:26.
939 [46] Angel SO, Vanagas L, Ruiz DM, Cristaldi C, Saldarriaga Cartagena AM, Sullivan WJJ. Emerging
940 Therapeutic Targets Against Toxoplasma gondii: Update on DNA Repair Response Inhibitors and
941 Genotoxic Drugs. Front Cell Infect Microbiol. 2020;10.
942 [47] Behnke MS, Fentress SJ, Mashayekhi M, Li LX, Taylor GA, Sibley LD. The polymorphic
943 pseudokinase ROP5 controls virulence in Toxoplasma gondii by regulating the active kinase ROP18.
944 PLoS pathogens. 2012;8:e1002992.
945 [48] Etheridge RD, Alaganan A, Tang K, Lou HJ, Turk BE, Sibley LD. The Toxoplasma pseudokinase
946 ROP5 forms complexes with ROP18 and ROP17 kinases that synergize to control acute virulence in
947 mice. Cell host & microbe. 2014;15:537-50.
948 [49] Reese ML, Zeiner GM, Saeij JP, Boothroyd JC, Boyle JP. Polymorphic family of injected
949 pseudokinases is paramount in Toxoplasma virulence. Proc Natl Acad Sci U S A. 2011;108:9625-30.
950 [50] Saeij JP, Boyle JP, Coller S, Taylor S, Sibley LD, Brooke-Powell ET, et al. Polymorphic secreted
951 kinases are key virulence factors in toxoplasmosis. Science. 2006;314:1780-3.
952 [51] Fentress SJ, Behnke MS, Dunay IR, Mashayekhi M, Rommereim LM, Fox BA, et al.
953 Phosphorylation of immunity-related GTPases by a Toxoplasma gondii-secreted kinase promotes
954 macrophage survival and virulence. Cell host & microbe. 2010;8:484-95.
955 [52] Wysocka J. Identifying novel proteins recognizing histone modifications using peptide pull-
956 down assay. Methods. 2006;40:339-43.

957 [53] Attar N, Campos OA, Vogelauer M, Cheng C, Xue Y, Schmollinger S, et al. The histone H3-H4
958 tetramer is a copper reductase enzyme. Science. 2020;369:59-64.
959 [54] Singh A, Verma S, Modak SB, Chaturvedi MM, Purohit JS. Extra-nuclear histones: origin,
960 significance and perspectives. Mol Cell Biochem. 2022;477:507-24.
961 [55] Choi YS, Hoon Jeong J, Min HK, Jung HJ, Hwang D, Lee SW, et al. Shot-gun proteomic analysis of
962 mitochondrial D-loop DNA binding proteins: identification of mitochondrial histones. Molecular
963 bioSystems. 2011;7:1523-36.
964 [56] Zanin MK, Donohue JM, Everitt BA. Evidence that core histone H3 is targeted to the
965 mitochondria in Brassica oleracea. Cell Biol Int. 2010;34:997-1003.
966 [57] Roson JN, Vitarelli MO, Costa-Silva HM, Pereira KS, Pires DDS, Lopes LS, et al. H2B.V demarcates
967 divergent strand-switch regions, some tDNA loci, and genome compartments in Trypanosoma cruzi
968 and affects parasite differentiation and host cell invasion. PLoS pathogens. 2022;18:e1009694.
969 [58] Croken MM, Nardelli SC, Kim K. Chromatin modifications, epigenetics, and how protozoan
970 parasites regulate their lives. Trends Parasitol. 2012;28:202-13.
971 [59] Croken MM, Qiu W, White MW, Kim K. Gene Set Enrichment Analysis (GSEA) of Toxoplasma
972 gondii expression datasets links cell cycle progression and the bradyzoite developmental program.
973 BMC genomics. 2014;15:515.
974 [60] Wang J, Dixon SE, Ting LM, Liu TK, Jeffers V, Croken MM, et al. Lysine acetyltransferase GCN5b
975 interacts with AP2 factors and is required for Toxoplasma gondii proliferation. PLoS pathogens.
976 2014;10:e1003830.
977 [61] Jeffers V, Gao H, Checkley LA, Liu Y, Ferdig MT, Sullivan WJ, Jr. Garcinol Inhibits GCN5-Mediated
978 Lysine Acetyltransferase Activity and Prevents Replication of the Parasite Toxoplasma gondii.
979 Antimicrobial agents and chemotherapy. 2016;60:2164-70.
980 [62] Huang S, Holmes MJ, Radke JB, Hong DP, Liu TK, White MW, et al. Toxoplasma gondii AP2IX-4
981 Regulates Gene Expression during Bradyzoite Development. mSphere. 2017;2.
982 [63] Khelifa AS, Guillen Sanchez C, Lesage KM, Huot L, Mouveaux T, Pericard P, et al. TgAP2IX-5 is a
983 key transcriptional regulator of the asexual cell cycle division in Toxoplasma gondii. Nature
984 communications. 2021;12:116.
985 [64] Sindikubwabo F, Ding S, Hussain T, Ortet P, Barakat M, Baumgarten S, et al. Modifications at
986 K31 on the lateral surface of histone H4 contribute to genome structure and expression in
987 apicomplexan parasites. eLife. 2017;6.
988 [65] Gissot M, Kelly KA, Ajioka JW, Greally JM, Kim K. Epigenomic modifications predict active
989 promoters and gene structure in Toxoplasma gondii. PLoS pathogens. 2007;3:e77.
990 [66] Ren Q, Gorovsky MA. Histone H2A.Z acetylation modulates an essential charge patch. Mol Cell.
991 2001;7:1329-35.
992 [67] Ren Q, Gorovsky MA. The nonessential H2A N-terminal tail can function as an essential charge
993 patch on the H2A.Z variant N-terminal tail. Mol Cell Biol. 2003;23:2778-89.
994 [68] Macadangdang BR, Oberai A, Spektor T, Campos OA, Sheng F, Carey MF, et al. Evolution of
995 histone 2A for chromatin compaction in eukaryotes. eLife. 2014;3.
996 [69] Severo V, Souza R, Vitorino F, Cunha J, Avila A, Arrizabalaga G, et al. Previously Unidentified
997 Histone H1-Like Protein Is Involved in Cell Division and Ribosome Biosynthesis in Toxoplasma gondii.
998 mSphere. 2022;7:e0040322.
999 [70] Sarah Sokol Borrelli SMR, Katherine G. Sharp, Leah F. Cabo, Hisham S. Alrubaye, Bruno
1000 Martorelli Di Genova and Jon P. Boyle. A transcriptional network required for Toxoplasma gondii
1001 tissue cyst formation is dispensable for long-term persistence. bioRxiv. 2022.
1002 [71] M. Haley Licon CJG, Sundeep Chakladar, Lindsey Shallberg, Benjamin S. Waldman, Christopher
1003 A. Hunter, Sebastian Lourido. A positive feedback loop controls Toxoplasma chronic differentiation.
1004 Biorxvi. 2022.

1005 [72] Colino-Sanguino Y, Cornett EM, Moulder D, Smith GC, Hrit J, Cordeiro-Spinetti E, et al. A
1006 Read/Write Mechanism Connects p300 Bromodomain Function to H2A.Z Acetylation. iScience.
1007 2019;21:773-88.
1008 [73] Afroz T, Cienikova Z, Clery A, Allain FHT. One, Two, Three, Four! How Multiple RRMs Read the
1009 Genome Sequence. Methods in enzymology. 2015;558:235-78.
1010 [74] Malumbres M. Cyclin-dependent kinases. Genome biology. 2014;15:122.
1011 [75] Jin C, Zang C, Wei G, Cui K, Peng W, Zhao K, et al. H3.3/H2A.Z double variant-containing
1012 nucleosomes mark 'nucleosome-free regions' of active promoters and other regulatory regions.
1013 Nature genetics. 2009;41:941-5.
1014 [76] Rahal R, Amon A. Mitotic CDKs control the metaphase-anaphase transition and trigger spindle
1015 elongation. Genes & development. 2008;22:1534-48.
1016 [77] Lukasik P, Zaluski M, Gutowska I. Cyclin-Dependent Kinases (CDK) and Their Role in Diseases
1017 Development-Review. International journal of molecular sciences. 2021;22.
1018 [78] Ors A, Papin C, Favier B, Roulland Y, Dalkara D, Ozturk M, et al. Histone H3.3 regulates mitotic
1019 progression in mouse embryonic fibroblasts. Biochemistry and cell biology = Biochimie et biologie
1020 cellulaire. 2017;95:491-9.
1021 [79] Page MJ, Di Cera E. Evolution of peptidase diversity. J Biol Chem. 2008;283:30010-4.
1022 [80] Harvey SH, Krien MJ, O'Connell MJ. Structural maintenance of chromosomes (SMC) proteins, a
1023 family of conserved ATPases. Genome biology. 2002;3:REVIEWS3003.
1024 [81] Laflamme G, Tremblay-Boudreault T, Roy MA, Andersen P, Bonneil E, Atchia K, et al. Structural
1025 maintenance of chromosome (SMC) proteins link microtubule stability to genome integrity. J Biol
1026 Chem. 2014;289:27418-31.
1027 [82] Serrano D, Cordero G, Kawamura R, Sverzhinsky A, Sarker M, Roy S, et al. The Smc5/6 Core
1028 Complex Is a Structure-Specific DNA Binding and Compacting Machine. Mol Cell. 2020;80:1025-38
1029 e5.
1030 [83] Borgogno MV, Monti MR, Zhao W, Sung P, Argarana CE, Pezza RJ. Tolerance of DNA Mismatches
1031 in Dmc1 Recombinase-mediated DNA Strand Exchange. J Biol Chem. 2016;291:4928-38.
1032 [84] Denkers EY, Gazzinelli RT. Regulation and function of T-cell-mediated immunity during
1033 Toxoplasma gondii infection. Clin Microbiol Rev. 1998;11:569-88.
1034 [85] Blader IJ, Saeij JP. Communication between Toxoplasma gondii and its host: impact on parasite
1035 growth, development, immune evasion, and virulence. APMIS. 2009;117:458-76.
1036 [86] Elsaid MM, Vitor RW, Frezard FJ, Martins MS. Protection against toxoplasmosis in mice
1037 immunized with different antigens of Toxoplasma gondii incorporated into liposomes. Mem Inst
1038 Oswaldo Cruz. 1999;94:485-90.
1039 [87] Sanchez-Lopez EF, Corigliano MG, Oliferuk S, Ramos-Duarte VA, Rivera M, Mendoza-Morales
1040 LF, et al. Oral Immunization With a Plant HSP90-SAG1 Fusion Protein Produced in Tobacco Elicits
1041 Strong Immune Responses and Reduces Cyst Number and Clinical Signs of Toxoplasmosis in Mice.
1042 Front Plant Sci. 2021;12:726910.
1043 [88] Buxton D, Innes EA. A commercial vaccine for ovine toxoplasmosis. Parasitology. 1995;110
1044 Suppl:S11-6.
1045 [89] Wu M, Liu S, Chen Y, Liu D, An R, Cai H, et al. Live-attenuated ME49Deltacdpk3 strain of
1046 Toxoplasma gondii protects against acute and chronic toxoplasmosis. NPJ Vaccines. 2022;7:98.
1047 [90] Echeverria PC, Matrajt M, Harb OS, Zappia MP, Costas MA, Roos DS, et al. Toxoplasma gondii
1048 Hsp90 is a potential drug target whose expression and subcellular localization are developmentally
1049 regulated. J Mol Biol. 2005;350:723-34.
1050 [91] Guzman F, Gauna A, Roman T, Luna O, Alvarez C, Pareja-Barrueto C, et al. Tea Bags for Fmoc
1051 Solid-Phase Peptide Synthesis: An Example of Circular Economy. Molecules. 2021;26.

1052 [92] Spiess PC, Deng B, Hondal RJ, Matthews DE, van der Vliet A. Proteomic profiling of acrolein
1053 adducts in human lung epithelial cells. J Proteomics. 2011;74:2380-94.

1054